involve
a journal of mathematics

Four-periodic infinite staircases for four-dimensional polydisks

Caden Farley, Tara S. Holm, Nicki Magill, Jemma Schroder, Zichen Wang, Morgan Weiler and Elizaveta Zabelina

msp

2025 vol. 18, no. 1

INVOLVE 18:1 (2025)
https://doi.org/10.2140/involve.2025.18.25

Four-periodic infinite staircases for four-dimensional polydisks

Caden Farley, Tara S. Holm, Nicki Magill, Jemma Schroder, Zichen Wang, Morgan Weiler and Elizaveta Zabelina

(Communicated by Frank Morgan)

The ellipsoid embedding function of a symplectic four-manifold measures the amount by which its symplectic form must be scaled in order for it to admit an embedding of an ellipsoid of varying eccentricity. This function generalizes the Gromov width and ball packing numbers. In the one continuous family of symplectic four-manifolds that has been analyzed, one-point blowups of the complex projective plane, there is an open dense set of symplectic forms whose ellipsoid embedding functions are completely described by finitely many obstructions, while there is simultaneously a Cantor set of symplectic forms for which an infinite number of obstructions are needed. In the latter case, we say that the embedding function has an infinite staircase. In this paper we identify a new infinite staircase when the target is a four-dimensional polydisk, extending a countable family identified by Usher (2019). Our work computes the function on infinitely many intervals and thereby indicates a method of proof for a conjecture of Usher.

1. Introduction

A *symplectic form* on a $2n$-dimensional smooth manifold X is a differential 2-form satisfying

- $d\omega = 0$, i.e., ω is closed, and
- $\omega^n \neq 0$, i.e., ω is nondegenerate.

MSC2020: 11A55, 53-04, 53D05, 53D35, 53D42.
Keywords: symplectic embeddings in four dimensions, ellipsoid embedding capacity function, infinite staircases, continued fractions, quantitative symplectic geometry, polydisks.

A symplectic form can be thought of as a skew-symmetric version of a Riemannian metric, providing area rather than length measurement. Symplectic geometry forms the mathematical framework for classical mechanics and is a go-between from Riemannian to complex geometry.

The *volume* $\mathrm{vol}(X)$ of a symplectic manifold is the quantity $\int_X \omega^n$. We say a smooth embedding $\varphi : (X, \omega) \to (X', \omega')$ is *symplectic* if $\varphi^*(\omega') = \omega$, and we denote a symplectic embedding by

$$\varphi : (X, \omega) \overset{s}{\hookrightarrow} (X', \omega'),$$

or $X \overset{s}{\hookrightarrow} X'$ when the symplectic form is clear from context and we are not emphasizing the specific embedding φ.

Let (X, ω) be a four-dimensional symplectic manifold. Its *ellipsoid embedding function*[1] is

$$c_X(z) := \inf\{\lambda \mid (E(1, z), \omega_0) \overset{s}{\hookrightarrow} (X, \lambda\omega)\}, \tag{1-0-1}$$

where $z \in \mathbb{R}_{>0}$, $\lambda X := (X, \lambda\omega)$ is X with the symplectic form scaled, the *ellipsoid* $E(c, d) \subset \mathbb{C}^2$ is the set

$$E(c, d) = \left\{ (\zeta_1, \zeta_2) \in \mathbb{C}^2 \;\middle|\; \pi\left(\frac{|\zeta_1|^2}{c} + \frac{|\zeta_2|^2}{d}\right) < 1 \right\},$$

and ω_0 is the standard symplectic form $dx_1 \wedge dy_1 + dx_2 \wedge dy_2$ on $\mathbb{C}^2$. Note that the associated volume form is twice the standard volume form on $\mathbb{R}^4$, thus $\mathrm{vol}(E(c, d)) = cd$. There is a symmetry that allows us to reduce to $z \geq 1$. Namely, for $0 < z < 1$, we have $c_X(z) = z c_X(1/z)$, because ω_0 restricted to $E(1, z)$ equals $z\omega_0$ restricted to $E(1/z, 1)$ under the diffeomorphism $(\zeta_1, \zeta_2) \mapsto (\zeta_1/\sqrt{z}, \zeta_2/\sqrt{z})$. Therefore, from now on we restrict the domain of $c_X(z)$ to $\mathbb{R}_{\geq 1}$.

The ellipsoid embedding function generalizes the Gromov width[2] via

$$c_{Gr}(X, \omega) = \frac{1}{c_X(1)},$$

and the fraction of the volume of X that can be filled by $n \in \mathbb{Z}_{\geq 1}$ equal balls can, by [McDuff 2009, Theorem 1.1], be computed from c_X via

$$\frac{n}{c_X(n)^2 \,\mathrm{vol}(X)}.$$

For a class of targets (X, ω) called "finite-type convex toric domains" (see Section 2.1), which includes the polydisks that we study, the ellipsoid embedding function satisfies several key properties.

[1] It is sometimes also called the *embedding capacity function* or *capacity function*.

[2] The *Gromov width* of a symplectic manifold is $\sup\{r \mid E(r, r) \overset{s}{\hookrightarrow} (X, \omega)\}$, or the largest ball that embeds into (X, ω).

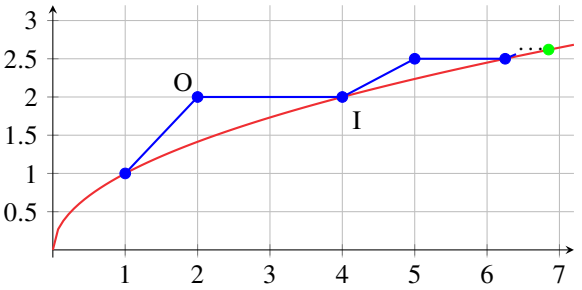

Figure 1. In blue, the graph of the embedding capacity function for a ball $X = B^4(1)$ is shown on the domain indicated. The graph in red is the volume lower bound established in Proposition 1.0.1 (i). The point marked O is an outer corner and the point marked I is an inner corner. This target has an ascending infinite staircase, first identified by McDuff and Schlenk [2012] and called the Fibonacci staircase in the literature. The accumulation point is green.

Proposition 1.0.1 [Cristofaro-Gardiner et al. 2020, p. 4, Proposition 2.1]. *Let (X, ω) be a finite-type convex toric domain. The ellipsoid embedding function $c_X(z)$ satisfies the following properties*:

(i) $c_X(z) \geq \sqrt{z/\mathrm{vol}(X)}$;

(ii) c_X *is nondecreasing*;

(iii) c_X *is* ***sublinear***: *for all $t \geq 1$, we have $c_X(tz) \leq t c_X(z)$*;

(iv) $c_X(z)$ *is continuous (in z)*;

(v) $c_X(z)$ *is equal to the volume curve for sufficiently large values of z; and*

(vi) $c_X(z)$ *is piecewise linear, when not equal to the volume curve and not at the limit of singular points.*

We say c_X or X has an *infinite staircase* if it is nonsmooth at infinitely many points. An *outer corner* is a nonsmooth point near which the function is concave while an *inner corner* is one near which the function is convex. By Proposition 1.0.1 (v), the set of nonsmooth points is bounded. By [Cristofaro-Gardiner et al. 2020, Theorem 1.13] (see Theorem 2.1.2 for a statement in our case), the nonsmooth points of c_X have a unique finite limit point called the *accumulation point*, whose z-coordinate we denote by $\mathrm{acc}(X)$. (By abuse of notation, we also refer to this z-coordinate as the "accumulation point".) We say an infinite staircase is *ascending* if the nonsmooth points accumulate from the left and *descending* if the nonsmooth points accumulate from the right. These concepts are illustrated in Figure 1. In this paper, we will establish the existence of an ascending staircase.

1.1. ***Summary of results.*** Our target of choice will be the *polydisk*, defined for $\beta \in \mathbb{R}_{\geq 1}$ by

$$P(1,\beta) := \{(\zeta_1,\zeta_2) \in \mathbb{C}^2 \mid \pi|\zeta_1|^2 \leq 1,\ \pi|\zeta_2|^2 \leq \beta\}.$$

We denote by c_β its ellipsoid embedding function $c_{P(1,\beta)}$. The polydisk is a finite-type convex toric domain, so c_β satisfies Proposition 1.0.1. In this case there are two functions,

$$\operatorname{acc}(\beta) := \operatorname{acc}(P(1,\beta)) : [1,\infty) \to [3+2\sqrt{2},\infty),$$
$$\operatorname{vol}(\beta) := \sqrt{\frac{\operatorname{acc}(\beta)}{\operatorname{vol}(P(1,\beta))}} : [1,\infty) \to \left[1+\tfrac{1}{2}\sqrt{2},1\right),$$

where, if c_β has an infinite staircase, its accumulation point has coordinates $(\operatorname{acc}(\beta), \operatorname{vol}(\beta))$ [Cristofaro-Gardiner et al. 2020, Theorem 1.13]; see Lemma 2.1.3.

The first ellipsoid embedding function was computed for $X = B^4 := E(1,1)$ in [McDuff and Schlenk 2012]. They found that its graph contained an infinite staircase whose inner and outer corners were derived from the Fibonacci numbers. Further work in [Frenkel and Müller 2015] exhibited a similar infinite staircase in c_1 governed by the Pell numbers, while on the other hand work of Cristofaro-Gardiner, Frenkel, and Schlenk showed that the property of having an infinite staircase is not universal: the functions c_n for $n \in \mathbb{Z}_{>1}$ do not contain infinite staircases [Cristofaro-Gardiner et al. 2017]. More generally, a conjecture of Cristofaro-Gardiner, Holm, Mandini, and Pires in [Cristofaro-Gardiner et al. 2020] suggests that c_β should not contain an infinite staircase for any rational β.

However, Usher [2019] suggested that the set of irrational β for which c_β has an infinite staircase might be quite rich: he identified a bi-infinite family $L_{n,k} \in \mathbb{R}_{\geq 1}$ for which the $c_{L_{n,k}}$ have infinite staircases.[3] Of particular interest to us are his

$$L_{n,0} := \sqrt{n^2-1}, \quad n \geq 2,$$

which generate the $k > 0$ values of L with infinite staircases (see Section 4.4). See Figure 2 for a visualization of these results via a plot of the relevant accumulation points.

Work by Bertozzi, Holm, Maw, McDuff, Mwakyoma, Pires, and Weiler [Bertozzi et al. 2021] and by Magill and McDuff [2023] proved an analogous result for the target

$$H_b := \{(\zeta_1,\zeta_2) \in \mathbb{C}^2 \mid \pi|\zeta_1|^2 + \pi|\zeta_2|^2 \leq 1,\ \pi|\zeta_2|^2 \leq 1-b\}.$$

[3] In this paper as well as in the closely related papers [Bertozzi et al. 2021; Magill and McDuff 2023; Magill et al. 2024], we use k to denote the staircase step and i to denote the image of a step, staircase, or b value under a symmetry analogous to Usher's Brahmagupta moves [Usher 2019, Definition 2.10]. Our notation differs from Usher's by switching what the i and k indices denote. We generally stick to our convention throughout but use Usher's convention here.

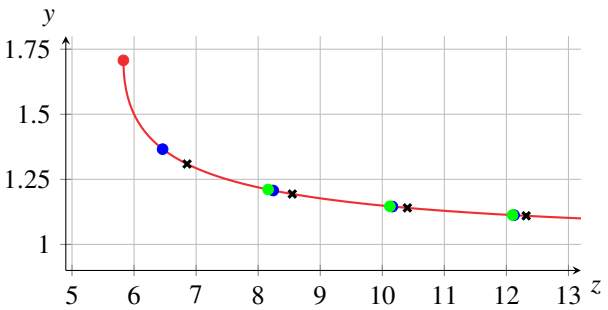

Figure 2. The parametrized curve $(\mathrm{acc}(\beta), \mathrm{vol}(\beta))$ is shown in red. The point on the curve at β represents a point at which an infinite staircase for c_β must accumulate, if it exists. The red dot is the accumulation point of the Pell stairs of Frenkel–Müller; the blue dots are the $L_{n,0}$ staircases of Usher; and the black $\times$s indicate values of β without infinite staircases, proved by Cristofaro-Gardiner, Frenkel, and Schlenk. The accumulation points of the new infinite staircases of Theorem 1.1.1 and Conjecture 1.1.2 are indicated by green dots.

(The region H_b is equivalent in terms of ellipsoid embeddings, see Section 2.1.1, to $\mathbb{C}P^2\#\overline{\mathbb{C}P}^2$, thus in the literature on infinite staircases it is also called the *Hirzebruch surface*.) They showed that there are two bi-infinite families $b_{n,i,\delta}$, with $n, i \in \mathbb{Z}_{\geq 0}$ and $\delta \in \{0, 1\}$, for which c_{H_b} has an ascending infinite staircase. Moreover, each ascending infinite staircase comes paired with a descending infinite staircase.

One feature that all infinite staircases described so far appear to have in common is that their outer corners are at z-values whose continued fractions grow by a predictable pattern of adding pairs of integers. Recall that real numbers can be described by their *continued fractions*, e.g.,

$$[m, n, \ell] = m + \frac{1}{n + 1/\ell},$$

with repeated parts denoted by

$$[m, \{n, \ell\}^k] = [m, \underbrace{n, \ell, \dots, n, \ell}_{k \text{ times}}], \qquad [m, \{n, \ell\}^\infty] = [m, n, \ell, n, \ell, n, \ell, \dots].$$

Every positive real number has a continued fraction with all entries positive integers; rational numbers have finite continued fractions, quadratic irrational numbers (irrational roots of quadratic equations with rational coefficients) have infinite periodic continued fractions, and nonquadratic irrational numbers have infinite nonperiodic continued fractions. We will abuse notation and occasionally allow the last entry in a finite continued fraction to be a real number, e.g., in the proof of Theorem 1.1.1 (ii) in Section 3.1. Doing so is just a matter of notation, because if $a_i \in \mathbb{Z}_{>0}$ and $z \in \mathbb{R}$ has continued fraction $[b_0, b_1, \dots]$ then $[a_0, \dots, a_n, z] = [a_0, \dots, a_n, b_0, b_1, \dots]$.

Allowing the last number to be real can be helpful when trying to understand the algebraic relationships among the continued fraction's rational approximations, as in Lemma 3.1.5.

Recall that an *outer corner* of c_X is a nonsmooth point near which c_X is convex; see Figure 11 on page 47. The outer corners of the Fibonacci stairs of McDuff–Schlenk have continued fractions

$$[2],\ [5],\ [6,1,5,2],\ [6,1,5,1,4],\ [6,1,5,1,5,2],\ [6,1,5,1,5,1,4],\ \ldots.$$

The accumulation points of all infinite staircases discussed so far are quadratic irrationals with two-periodic continued fractions. We say an infinite staircase is $2m$*-periodic* if the continued fraction of the k-th outer corner equals that of the $(k-2)$-th outer corner with a fixed length $2m$ sequence of integers added after a fixed sequence of integers at the beginning. For example, in the sequence above, the Fibonacci stairs are 2-periodic with a pair $1, 5$ inserted recursively after the 6.

In [Magill et al. 2024], Magill, McDuff, and Weiler showed that, between each of the pairs of adjacent ascending and descending infinite staircases studied in [Bertozzi et al. 2021; Magill and McDuff 2023], there is a further Cantor set of values of b for which c_{H_b} has an infinite staircase. These include infinite staircases whose outer corners and accumulation points appear to have higher-periodic continued fractions, as well as infinite staircases whose accumulation points may not be quadratic irrational. They were obtained by generalizing the procedure to construct an infinite staircase whose outer corners have four-periodic continued fractions accumulating to $[\{7,5,3,1\}^\infty]$ from the descending staircase accumulating to $[7,\{5,1\}^\infty]$ and the ascending staircase accumulating to $[\{7,3\}^\infty]$.

We predict a very close correspondence between the cases of the polydisk and H_b in Conjecture 1.2.1. Our main theorem provides evidence for this conjecture.

Theorem 1.1.1. *Set*

$$\beta = \tfrac{1}{12}(6+5\sqrt{30}).$$

(i) *The function c_β has an infinite staircase.*

(ii) *It is four-periodic, with* $\operatorname{acc}(\beta) = [\{8,6,4,2\}^\infty]$.

See Figure 3 for a visualization. Detail on the location of the accumulation point of the infinite staircase of Theorem 1.1.1 is given in Figure 4.

Of note is the fact that we prove Theorem 1.1.1 in Section 3 by computing it on infinitely many intervals. In Section 3 we also outline a procedure for computing c_β on the entire interval $[1, \operatorname{acc}(\beta)]$ containing the infinite staircase. This would prove an analogue of [Usher 2019, Conjecture 4.23], with the role of his A classes being played by our $\boldsymbol{E}$ classes and his $\hat{A}$ classes replaced by our $\hat{\boldsymbol{E}}$ classes: see the preamble to Section 3 for the definitions $\boldsymbol{E}$ and $\hat{\boldsymbol{E}}$, and see Section 4.2 for further discussion of Usher's conjecture.

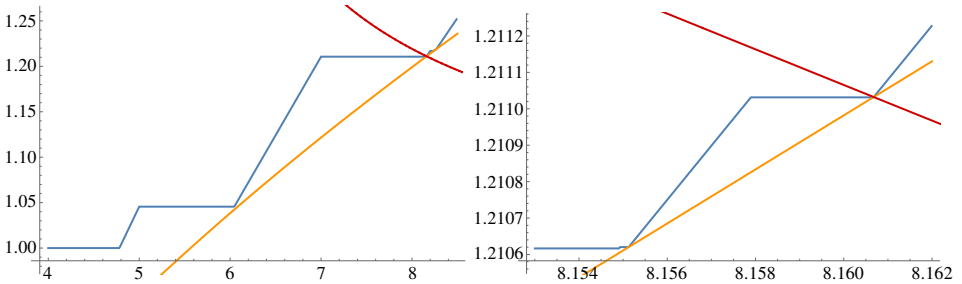

Figure 3. Here we depict the infinite staircase c_β of Theorem 1.1.1. In both figures, with β as in Theorem 1.1.1, the orange curve is $\mathrm{vol}_\beta(z)$ and c_β is in blue. The accumulation point curve $(\mathrm{acc}(\beta), \mathrm{vol}(\beta))$ is in red — for this curve, β varies. Thus the accumulation point of c_β occurs at the intersection of these three curves. On the right, we have zoomed in; the obstructions from $\boldsymbol{E}_0$, $\hat{\boldsymbol{E}}_1$, and $\boldsymbol{E}_2$ are visible. See Sections 2.2 and 3 for definitions.

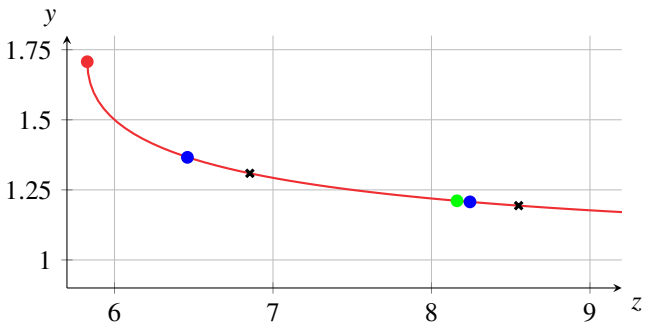

Figure 4. This figure uses the same color scheme as Figure 2. More detail near the infinite staircase of Theorem 1.1.1 is shown. The new staircase's accumulation point is the green dot, while the two blue dots are Usher's staircases with $\beta = L_{2,0}$ and $L_{3,0}$.

From experimental evidence and by combining Conjecture 1.1.2 with [Magill et al. 2024, Theorem 1.1.1], we furthermore expect that our result generalizes to all $n \in \mathbb{Z}_{\geq 2}$.

Conjecture 1.1.2. *Let β_n be of the form*

$$\beta_n = \tfrac{1}{2} + \frac{(2n+1)\sqrt{n(n^3+2n^2-1)}}{2n(n+1)},$$

with $n \in \mathbb{Z}_{\geq 2}$.

(i) *The function c_{β_n} has an infinite staircase.*

(ii) *It is four-periodic, with* $\mathrm{acc}(\beta_n) = [\{2n+4, 2n+2, 2n, 2n-2\}^\infty]$.

Note that setting $n = 2$ in Conjecture 1.1.2 reduces to Theorem 1.1.1.

1.2. ***Connections to other targets.*** There is a function

$$\mathrm{acc}_H : [0, 1) \to [3 + 2\sqrt{2}, \infty)$$

which is analogous to acc in the following way: if c_{H_b} has an infinite staircase then $\mathrm{acc}_H(b)$ is the z-coordinate of its accumulation point. It is two-to-one in general, but when restricted to $\left[\frac{1}{3}, 1\right)$, it is one-to-one with range $[3+2\sqrt{2}, \infty)$. These facts have a similar proof to Lemma 2.1.3.

Conjecture 1.2.1. *Define a function $f : \mathbb{R} \to \mathbb{R}$ by sending z to the number whose continued fraction is obtained from the continued fraction of z by subtracting one from each entry.*

Let $\beta \geq \sqrt{3}$. The function c_β has an infinite staircase if and only if the function c_{H_b} has an infinite staircase, where

$$b = \mathrm{acc}_H^{-1} \circ f \circ \mathrm{acc}(\beta).$$

The infinite staircases $c_{L_{n,0}}$ of [Usher 2019], c_{β_n} of Conjecture 1.1.2, and the fact that c_n, $n \in \mathbb{Z}$, do not contain infinite staircases from [Cristofaro-Gardiner et al. 2017] all support Conjecture 1.2.1. Further evidence is explored in [Magill et al. 2023, §3 and Remark 3.1.7]. It is possible to extend Conjecture 1.2.1 to all β using the Brahmagupta moves of Usher and their counterparts for the Hirzebruch surface from [Magill and McDuff 2023]; explaining the extension is beyond the scope of this paper. Because of the similarities between Section 3.2 and [Magill 2024], we expect there is a more direct relationship between b and β than via the accumulation point function acc, but this has not yet been discovered.

In Section 3.2, to construct the desired embeddings, we followed the sequences of mutations on almost toric fibrations found by Magill [2024; ≥ 2025]. In [Magill 2024], ATF mutations for ellipsoid embeddings into H_b were considered. The formulas found for the mutations in Section 3.2 mirror the formulas found in [Magill 2024]. In fact, the formulas in Lemmas 3.2.9 and 3.2.12 could be easily generalized to mirror the formulas of [Magill 2024, Definition 3.8]. Therefore, we expect a generalization of Proposition 3.2.10 similar to [Magill 2024, Theorem 1.1]. This is more evidence for the correspondence between the embedding functions for polydisks and H_b.

In [Magill ≥ 2025], ellipsoid embeddings into a two-fold blowup of $\mathbb{C}P^2$ were considered. In Section 3.2, we follow the same mutation sequences Magill used to compute some of the inner corners of the function. One new addition in Section 3.2 is Conjecture 3.0.7 that adding one extra mutation to Magill's sequences will compute all the inner corners of the function for c_β. The work of Casals and Vianna [2022] and Cristofaro-Gardiner, Holm, Mandini, and Pires in [Cristofaro-Gardiner et al. 2020] shows that almost toric mutations give all embeddings for particular rational convex

toric domains. Conjecture 3.0.7 would imply a similar statement holds for c_β, where $\beta = \frac{1}{12}(6+5\sqrt{30})$. It would be interesting to see if similar statements hold for H_b and the two-fold blowup of $\mathbb{C}P^2$.

1.3. ***Outline of the paper.*** We introduce the necessary tools to analyze c_β in Section 2, prove Theorem 1.1.1 in Section 3, and in Section 4 we outline future work supported by other experimental evidence discovered in summer 2022. We discuss the Python code used in our experiments in the online supplement. Section 2.1.1 requires a graduate-level background in geometry and can be skipped on a first reading.

2. Tools for obstructing and constructing embeddings

In this section we define the tools we use to prove Theorem 1.1.1.

2.1. ***Embedding functions of toric domains.*** A *toric domain* X_Ω in $\mathbb{C}^2$ is the preimage of a domain $\Omega \subset \mathbb{R}^2_{\geq 0}$ under the map $\mu : \mathbb{C}^2 \to \mathbb{R}^2$ given by

$$(\zeta_1, \zeta_2) \mapsto (\pi|\zeta_1|^2, \pi|\zeta_2|^2).$$

We call the map μ the *moment map* and the domain Ω the *moment polygon* of X_Ω, as they are analogous to the moment maps and moment polygons associated to closed toric symplectic manifolds. We say that a toric domain X_Ω is *convex* if the domain Ω is a closed, connected region of $\mathbb{R}^2$ and is convex as a polygon in $\mathbb{R}^2$. As a consequence of the presence of factors of π in the expression for the moment map μ, the volume of a toric domain X_Ω coincides with twice the area of its moment polygon Ω.

When $(X, \omega) = (X_\Omega, \omega_0)$, instead of (1-0-1), we write

$$c_X(z) := \inf\{\lambda \mid E(1, z) \overset{s}{\hookrightarrow} X_{\lambda\Omega}\},$$

dropping the symplectic forms from the notation.

We say that a convex toric domain X_Ω is of *finite type* if Ω has only finitely many sides and all of these sides have rational slopes. For these finite-type toric domains, the accumulation points of potential infinite staircases can be computed as solutions to an explicit quadratic equation. For details of this result and the following definition, see [Cristofaro-Gardiner et al. 2020].

Definition 2.1.1. Let L be a line segment in $\mathbb{R}^2$. The *affine length* of L is the length of the image $AT(L)$ of L under a composition of a translation T with a linear transformation $A \in \mathrm{SL}(2, \mathbb{Z})$, where A and T are chosen so that $AT(L)$ lies along the x-axis.

If Ω is a polygon in $\mathbb{R}^2_{\geq 0}$ with only finitely many sides each of which has a rational slope, define the *affine perimeter* of Ω to be the sum of the affine lengths of its sides, and denote this quantity by $\mathrm{per}(\Omega)$.

With these definitions, we can now state the following result about the accumulation points of infinite staircases of finite-type convex toric domains.

Theorem 2.1.2 [Cristofaro-Gardiner et al. 2020, Theorem 1.13]. *Let X_Ω be a finite-type convex toric domain. If the ellipsoid embedding function $c_{X_\Omega}(z)$ has an infinite staircase, then it accumulates at $\mathrm{acc}(\Omega) \geq 1$, a real solution[4] to the quadratic equation*

$$z^2 - \left(\frac{\mathrm{per}(\Omega)^2}{2 \cdot \mathrm{area}(\Omega)} - 2\right) z + 1 = 0.$$

In this case, at $\mathrm{acc}(\Omega)$, the ellipsoid embedding function touches the volume curve:

$$c_{X_\Omega}(\mathrm{acc}(\Omega)) = \sqrt{\frac{\mathrm{acc}(\Omega)}{2 \cdot \mathrm{area}(\Omega)}}.$$

In the setting of this paper, X_Ω will be the polydisk $P(1, \beta)$, which has moment polygon Ω_β a rectangle situated at the origin with sides of length 1 and β parallel to the x- and y-axes. Here, the affine perimeter of Ω_β is the same as its regular perimeter, $\mathrm{per}(\Omega_\beta) = 2(\beta + 1)$, and the area of Ω_β is $\mathrm{area}(\Omega_\beta) = b$. In this case, the quadratic equation in Theorem 2.1.2 becomes

$$z^2 - \left(\frac{2(\beta+1)^2}{\beta} - 2\right) z + 1 = 0. \tag{2-1-1}$$

Besides providing an explicit way to calculate accumulation points, Theorem 2.1.2 also describes a necessary condition for the existence of an infinite staircase for different values of β. We call the difference $c_{X_\Omega}(\mathrm{acc}(\Omega)) - \sqrt{\mathrm{acc}(\Omega)/(2 \cdot \mathrm{area}(\Omega))} \geq 0$ the *staircase obstruction* of X_Ω. Theorem 2.1.2 indicates that if the ellipsoid embedding function $c_{X_\Omega}(z)$ has an infinite staircase, then the staircase obstruction of X_Ω vanishes. For the case where $X_\Omega = P(1, \beta)$, if the staircase obstruction does not vanish for a particular value of β, we say that this β-value is *blocked*, and we conclude that the ellipsoid embedding function $c_\beta(z)$ does not have an infinite staircase.

Finally, because the accumulation point of an infinite staircase is on the volume obstruction, the formula on the right-hand side of Proposition 1.0.1 (i) specialized to the case of the polydisk will be key throughout; we set the notation

$$\mathrm{vol}_\beta(z) := \sqrt{\frac{z}{2\beta}} = \sqrt{\frac{z}{2 \cdot \mathrm{area}(\Omega_\beta)}}.$$

We compute the ranges of acc and vol to motivate Figures 2 and 4.

[4]The solutions to this equation have product 1 and are either positive or complex. For the polydisk, there is always a unique real solution larger than one.

Lemma 2.1.3. *Setting* $\mathrm{acc}(\beta) = \mathrm{acc}(\Omega_\beta)$, *we have*

$$\mathrm{acc} : [1, \infty) \to [3 + 2\sqrt{2}, \infty),$$

and acc *is increasing. If we set* $\mathrm{vol}(\beta) = \mathrm{vol}_\beta(\mathrm{acc}(\beta))$ *then*

$$\mathrm{vol} : [1, \infty) \to \left[1 + \tfrac{1}{2}\sqrt{2}, 1\right),$$

and vol *is decreasing.*

Proof. Solving (2-1-1) we obtain

$$\mathrm{acc}(\beta) = z = \beta + 1 + \frac{1}{\beta} + \sqrt{\beta^2 + 2\beta + 2 + \frac{2}{\beta} + \frac{1}{\beta^2}},$$

thus

$$\mathrm{acc}(1) = 3 + \sqrt{8} = 3 + 2\sqrt{2},$$

and $\lim_{\beta\to\infty} \mathrm{acc}(\beta) = \infty$ because $\mathrm{acc}(\beta) > \beta$. The function $\mathrm{acc}(\beta)$ is increasing because

$$\frac{\partial}{\partial\beta}\left(\beta + 1 + \frac{1}{\beta}\right) = 1 - \frac{1}{\beta^2}$$

and

$$\frac{\partial}{\partial\beta}\left(\beta^2 + 2\beta + 2 + \frac{2}{\beta} + \frac{1}{\beta^2}\right) = 2\beta + 2 - \frac{2}{\beta^2} - \frac{2}{\beta^3},$$

which are both positive if $\beta > 1$.

Because $\mathrm{vol}_\beta(z)$ has β in the denominator, it is decreasing if z is increasing, so $\mathrm{vol}(\beta)$ is decreasing in β. We compute

$$\left(1 + \tfrac{1}{2}\sqrt{2}\right)^2 = 1 + \sqrt{2} + \tfrac{1}{2} = \tfrac{1}{2}(3 + 2\sqrt{2}) = \sqrt{\tfrac{1}{2}\mathrm{acc}(1)} = \mathrm{vol}(1).$$

Finally, by the fact that vol and acc are continuous and defined on $[1, \infty)$,

$$\begin{aligned}\left(\lim_{\beta\to\infty} \mathrm{vol}(\beta)\right)^2 &= \lim_{\beta\to\infty} \frac{\beta + 1 + \frac{1}{\beta} + \sqrt{\beta^2 + 2\beta + 2 + \frac{2}{\beta} + \frac{1}{\beta^2}}}{2\beta} \\ &= \lim_{\beta\to\infty} \frac{1}{2} + \frac{1}{2\beta} + \frac{1}{2\beta^2} + \sqrt{\frac{1}{4} + \frac{1}{2\beta} + \frac{1}{2\beta^2} + \frac{1}{2\beta^3} + \frac{1}{4\beta^4}} = 1. \quad \square\end{aligned}$$

2.1.1. *Closed toric symplectic manifolds.* Our methods rely on the fact that ellipsoid embeddings into certain finite-type convex toric domain targets are equivalent to ellipsoid embeddings into certain closed symplectic manifolds, specifically toric blowups of $\mathbb{C}P^2$. Topologically, *symplectic blowup* is a procedure where an open ball is removed from a manifold, and the resulting boundary sphere is collapsed along the Hopf fibration. This can be achieved in a symplectic manner if the ball was symplectically embedded; see [McDuff and Salamon 2017, Theorem 7.1.21]. In the special case when the initial manifold M is four-dimensional, the symplectic blowup procedure is equivalent to the symplectic connected sum $M\#\overline{\mathbb{C}P}^2$;

see [McDuff and Salamon 2017, Example 7.1.4]. Moreover, when M is a four-dimensional toric symplectic manifold and the blowup respects the action, then at the level of moment polygons, the toric blowup has the impact of truncating a vertex [McDuff and Salamon 2017, Example 7.1.15].

Toric symplectic manifolds are classified by their moment polytope, up to equivariant symplectomorphism of the manifold and up to affine equivalence of the polytopes. Those polytopes which are the moment polytope of some toric symplectic manifold are called *Delzant polytopes*. For four-dimensional toric symplectic manifolds, Delzant polygons are those that have edges with rational slope and, for each vertex, the two primitive vectors pointing in the directions of the edges form a $\mathbb{Z}$-basis of the integer lattice in $\mathbb{R}^2$. Because we work up to affine equivalence of Delzant polytopes, we may assume that a Delzant polygon has a vertex at the origin, that the edges emanating from the origin point along the positive x- and y-axes, and the polygon is contained in the positive quadrant. *Almost toric fibrations*, defined in Section 2.4, and natural operations on them allow us to modify the Delzant polygon of M_Ω to indicate new fibrations. We use the modified Delzant polygon to identify new embeddings $E(c,d) \overset{s}{\hookrightarrow} M_\Omega$ and [Cristofaro-Gardiner et al. 2020, Theorem 1.4], stated below, to prove there is thus an embedding into X_Ω.

Proposition 2.1.4 [Cristofaro-Gardiner et al. 2020, Theorem 1.4]. *If M_Ω is the toric symplectic manifold with Delzant polygon Ω, then*

$$E(c,d) \overset{s}{\hookrightarrow} M_\Omega \quad \Longleftrightarrow \quad E(c,d) \overset{s}{\hookrightarrow} X_\Omega.$$

2.2. ***Quasiperfect Diophantine classes.*** Embeddings of rational ellipsoids into finite-type convex toric domains are completely characterized by the homology classes of symplectically immersed spheres in blowups of $\mathbb{C}P^2$, a method due to McDuff and Polterovich (see the proof of [McDuff 2011, Proposition 3.2] and the original reference of [McDuff and Polterovich 1994]). We will not review this entire story, but refer the reader to the original proof, the in-depth survey [Hutchings 2011b] for the case of ellipsoid targets, or the shorter, more general summary in [Cristofaro-Gardiner et al. 2020, §2.3]. Here we make the definitions and simplifications used in this paper.

Define the *integral weight expansion* $W(p,q)$ of a pair of coprime integers $p > q$ recursively by

$$W(q,p) = W(p,q) = (q) \cup W(p-q,q)$$

and the *weight expansion* $\boldsymbol{w}(z)$ of a rational number $z = p/q$ to be

$$\boldsymbol{w}(z) := W(p,q)/q.$$

The *weights* of z are the entries in its weight expansion. Irrational numbers also have (infinite) weight expansions $\boldsymbol{w}(z) := W(z,1)$.

Example 2.2.1. We compute

$$W(41,5) = (5) \cup W(36,5) = (5,5) \cup W(31,5) = \cdots = (5^{\times 8}) \cup W(5,1) = (5^{\times 8}, 1^{\times 5}),$$

thus $\boldsymbol{w}(41/5) = (1^{\times 8}, (1/5)^{\times 5})$.

Remark 2.2.2. (i) The continued fraction of z equals the list of multiplicities of its weights, e.g.,

$$[8,5] = 8 + \tfrac{1}{5} = \tfrac{41}{5}.$$

(ii) By [McDuff and Schlenk 2012, Lemma 1.2.6], if $\boldsymbol{w}(p/q) = (w_1, \ldots, w_M)$, then

$$\sum_{i=1}^{M} w_i^2 = \frac{p}{q}, \quad \sum_{i=1}^{M} w_i = \frac{p}{q} + 1 - \frac{1}{q}.$$

Definition 2.2.3. We call a 5-tuple of integers

$$\boldsymbol{E} = (d, e, p, q, t)$$

with p and q coprime a *quasiperfect Diophantine class* if

$$2(d+e) = p+q, \quad 2de = pq - 1, \quad t = \sqrt{p^2 + q^2 - 6pq + 8}. \tag{2-2-1}$$

We say p/q is the *center* of $\boldsymbol{E}$, and call the first two equations in (2-2-1) the *Diophantine equations*.

Let $\mu_{\boldsymbol{E},\beta}$ be the obstruction function defined by

$$\mu_{\boldsymbol{E},\beta}(z) := \frac{W(p,q) \cdot \boldsymbol{w}(z)}{d + e\beta}.$$

Our computations in Section 3 will rely on the fact that

$$c_\beta(z) \geq \mu_{\boldsymbol{E},\beta}(z) \tag{2-2-2}$$

for all quasiperfect Diophantine classes $\boldsymbol{E}$. This follows from the fact that $\boldsymbol{E}$ represents the homology class of a symplectically immersed sphere in a blowup of $\mathbb{C}P^2$; the fact that the immersion is symplectic means the sphere has positive area, providing us with an inequality. For the purposes of this paper, (2-2-2) may be taken as a black box following from [McDuff 2011, Proposition 3.2].

Remark 2.2.4. (i) Computing $\mu_{\boldsymbol{E},\beta}$ at the center of $\boldsymbol{E}$ is particularly simple by Remark 2.2.2 (ii):

$$\mu_{\boldsymbol{E},\beta}\left(\frac{p}{q}\right) = \frac{q\,\boldsymbol{w}(p/q) \cdot \boldsymbol{w}(p/q)}{d + e\beta} = \frac{p}{d + e\beta}. \tag{2-2-3}$$

Many outer corners of c_β, including those in the infinite staircase of Theorem 1.1.1, have z-values equal to centers of quasiperfect Diophantine classes, and near those centers $c_\beta(z) = \mu_{\boldsymbol{E},\beta}(z)$.

(ii) The fact that t is an integer is redundant:

$$t^2 = 4(d+e)^2 - 16de = 4(d-e)^2.$$

Finally, we have the following identities relating d, e, p, q, and t:

Lemma 2.2.5. *An integral tuple $(d, e; p, q, t)$ is a quasiperfect Diophantine class if and only if t is defined from p and q as in (2-2-1) and there are integers (d, e) such that*

$$4d = p+q+t \quad \text{and} \quad 4e = p+q-t.$$

Proof. Using the linear Diophantine equation (2-2-1), we solve for e:

$$e = \tfrac{1}{2}(p+q) - d.$$

We then plug this into the quadratic Diophantine equation, giving us

$$\begin{aligned} d(p+q-2d) = pq-1 \quad &\iff \quad 2d^2 - d(p+q) + (pq-1) = 0 \\ &\iff \quad d = \tfrac{1}{4}(p+q+\sqrt{(p+q)^2 - 8(pq-1)}) \\ &\iff \quad 4d = p+q+t, \end{aligned}$$

using the fact that $d > e$. The formula for e follows in exactly the same way, using the fact that $e < d$ to obtain the other solution in the quadratic formula. □

2.3. ***ECH capacities.*** Another way to obtain a lower bound on the ellipsoid embedding function of a symplectic manifold is through embedded contact homology (ECH). Computing these lower bounds is algorithmic, and so allows us to explore the space of ellipsoid embedding functions c_β efficiently. In Lemma 2.3.5 we relate ECH obstructions to quasiperfect Diophantine classes.

Defined in [Hutchings 2011a], the *ECH capacities* of a convex toric domain X_Ω form a sequence

$$0 = c_0(X_\Omega) < c_1(X_\Omega) \le c_2(X_\Omega) \le \cdots \le \infty,$$

which obstruct symplectic embeddings:

$$X_\Omega \overset{s}{\hookrightarrow} X_{\Omega'} \quad \Longrightarrow \quad c_k(X_\Omega) \le c_k(X_{\Omega'}) \text{ for all } k.$$

Our computation of ECH capacities for $P(1, \beta)$ is based on [Cristofaro-Gardiner 2019, Appendix A].

Definition 2.3.1. A *convex lattice path* $\Lambda : [0, 1] \to \mathbb{R}_{\ge 0}$ is a continuous map satisfying

(1) piecewise linearity,

(2) all *vertices* (nonsmooth points) lie in $\mathbb{Z}^2$,

(3) $\Lambda(0)$ is on the y-axis and $\Lambda(a)$ is on the x-axis,

(4) the region enclosed by Λ and the axes is convex.

Its *edges* are the vector differences between adjacent vertices.

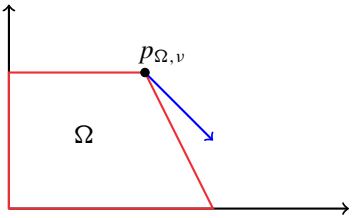

Figure 5. With Ω the region outlined in red and ν in blue, the black point is $p_{\Omega,\nu}$.

The function $\mathcal{L}(\Lambda)$ counts the number of lattice points enclosed by Λ, which includes points on $\partial\Lambda$ and those lying on the axes. We further define the Ω-*length* $\ell_\Omega(\Lambda)$ of a given path Λ as

$$\sum_{\nu\in\text{Edges}(\Lambda)} \det[\nu p_{\Omega,\nu}],$$

where $p_{\Omega,\nu}\in\partial\Omega$ is the unique point where ν, shifted to be based at $p_{\Omega,\nu}$, is tangent to $\partial\Omega$ and where Ω lies entirely to the right-hand side of ν. See Figure 5.

Theorem 2.3.2 [Cristofaro-Gardiner 2019, Corollary A.5]. *If X_Ω is a convex toric domain, then*

$$c_k(X_\Omega) = \min\{\ell_\Omega(\Lambda) : \textit{convex lattice paths } \Lambda \textit{ where } \mathcal{L}(\Lambda) = k+1\}.$$

The ECH capacities of an ellipsoid $E(a,b)$ can also be computed as follows.

Proposition 2.3.3 [Hutchings 2011a, Proposition 1.2]. *Let $N(a,b)$ be the sequence of elements of the array $(am+bn)_{m,n\in\mathbb{N}}$ listed in ascending order with repetitions. The k-th element indexed from zero of this sequence, $N_k(a,b)$, is exactly equal to $c_k(E(a,b))$.*

The use of ECH capacities to obstruct symplectic embeddings of ellipsoids into some target relies on the following result of Frenkel–Müller and Hutchings, which is also a special case of a theorem of Cristofaro-Gardiner.

Theorem 2.3.4 [Cristofaro-Gardiner 2019, Theorem 1.2; Frenkel and Müller 2015, Corollary 1.5; Hutchings 2011b, Corollary 11]. *There exists a symplectic embedding*

$$E(1,z) \overset{s}{\hookrightarrow} P(1,\beta)$$

if and only if

$$c_k(E(1,z)) \le c_k(P(1,\beta))$$

for all $k\in\mathbb{Z}_{\ge 0}$.

Since our target is $P(1,\beta)$, which is convex, we use the methods of [Bertozzi et al. 2021, §5] as well as Theorems 2.3.2, 2.3.4 and Proposition 2.3.3 to compute a lower bound for c_β. We identify $(P(1,\beta),\lambda\omega_0) = (P(\lambda,\lambda\beta),\omega_0)$ by the diffeomorphism $(\zeta_1,\zeta_2)\mapsto(\sqrt{\lambda}\zeta_1,\sqrt{\lambda}\zeta_2)$. Then

$$\begin{aligned}
\lambda \geq c_\beta(z) \quad &\iff \quad E(1,z) \overset{s}{\hookrightarrow} P(\lambda,\lambda\beta) \\
&\iff \quad c_k(E(1,z)) \leq c_k(P(\lambda,\lambda\beta)) \qquad \text{for all } k \\
&\iff \quad c_k(E(1,z)) \leq \lambda\cdot c_k(P(1,\beta)) \qquad \text{for all } k \\
&\iff \quad \frac{c_k(E(1,z))}{c_k(P(1,\beta))} \leq \lambda \qquad \text{for all } k,
\end{aligned}$$

where the third line follows by the conformality of ECH capacities [Hutchings 2011a, (2.5)]. Because $c_\beta(z)$ is the infimum over all such λ, we obtain

$$c_\beta(z) = \sup_k \frac{c_k(E(1,z))}{c_k(P(1,\beta))}. \tag{2-3-1}$$

It is (2-3-1) which allows us to explore the space of functions c_β for potential infinite staircases and identify our values in Theorem 1.1.1 and Conjecture 1.1.2 by computing

$$\max_{k\leq K} \frac{c_k(E(1,z))}{c_k(P(1,\beta))} \leq c_\beta(z) \tag{2-3-2}$$

for K large (e.g., $K = 25,000$ or $100,000$). The maximum in (2-3-2) is a good approximation for c_β when K is large by [Cristofaro-Gardiner et al. 2015, Theorem 1.1].

We can use ECH capacities to identify outer corners of c_β. Complementary to (2-2-3) and (2-2-2), we can use individual convex lattice paths, Theorem 2.3.2, and (2-3-1) to compute precise lower bounds to values of c_β at specific values of z. That is, to prove

$$c_\beta(z) \geq \lambda,$$

it is enough to find a single lattice path Λ for which $N_k(1,z)/\ell_{\Omega_\beta}(\Lambda) = \lambda$; see Remark 3.1.3. This is the method used in [Cristofaro-Gardiner et al. 2020].

However, in order to make use of [Magill 2024], we prove Theorem 1.1.1 using quasiperfect Diophantine classes rather than ECH capacities. Analogously to [Bertozzi et al. 2021, Lemma 92], we may translate between these perspectives.

Lemma 2.3.5. *If $\boldsymbol{E} = (d,e,p,q,t)$ is a quasiperfect Diophantine class, then*

$$\mu_{\boldsymbol{E},\beta}\left(\frac{p}{q}\right) \leq \frac{c_k(E(1,p/q))}{c_k(P(1,\beta))},$$

where $k = (d+1)(e+1)-1 = \frac{1}{2}(p+1)(q+1)-1$.

Lemma 2.3.5 allows us to translate between the obstructions from ECH capacities, which are algorithmic and thus good tools for analyzing c_β visually by Theorem 2.3.2 (see Figures 14 and 16), and quasiperfect Diophantine classes, which carry more information. Note that if $c_\beta(p/q) = \mu_{\boldsymbol{E},\beta}(p/q)$ then the conclusion of Lemma 2.3.5 is an equality.

Proof. It suffices to provide a lattice path $\Lambda_{\boldsymbol{E}}$ with $\mu_{\boldsymbol{E},\beta}(z) \le N_k(1,z)/\ell_{\Omega_\beta}(\Lambda_{\boldsymbol{E}})$: this is simply the rectangle with corners the origin, $(0,e)$, (d,e), and $(d,0)$. We check the conclusions of the lemma.

Firstly,

$$(d+1)(e+1) = \tfrac{1}{2}(p+1)(q+1) \quad \iff \quad 2de+2(d+e)+1 = pq+p+q+1,$$

which follows from (2-2-1).

Secondly, the edges of $\Lambda_{\boldsymbol{E}}$ are $(d,0)$ and $(0,-e)$. For both, we may use $p_{\Omega_\beta,\nu} = (\beta,1)$. Thus

$$\ell_{\Omega_\beta}(\Lambda_{\boldsymbol{E}}) = \det\begin{pmatrix} d & \beta \\ 0 & 1 \end{pmatrix} + \det\begin{pmatrix} 0 & \beta \\ -e & 1 \end{pmatrix} = d + e\beta,$$

which is the denominator of $\mu_{\boldsymbol{E},\beta}$.

Finally, it remains to show that $N_k(1, p/q) = W(p,q)\cdot \boldsymbol{w}(p/q) = p$. Identify the nonnegative integer linear combinations of 1 and $z = p/q$ with lattice points in $\mathbb{Z}^2_{\ge 0}$. We will show that if (x_0, y_0) is either $(p,0)$ or $(0,q)$, there are exactly $k = \frac{1}{2}(p+1)(q+1)-1$ lattice points in the first quadrant with $x+py/q < x_0+py_0/q$, and thus $N_k(1, p/q) = x_0 + py_0/q = p$.

Let T be the triangle below the line $x + py/q < p$ and above the axes. If I denotes the number of interior points of T and B its number of boundary points, the number of lattice points in the first quadrant below the line $x + py/q < p$ is $I + B - 2$. By Pick's theorem applied to T,

$$I+\tfrac{1}{2}B-1 = \tfrac{1}{2}pq \quad \iff \quad I+B-2 = \tfrac{1}{2}pq-1+\tfrac{1}{2}B = \tfrac{1}{2}pq-1+\tfrac{1}{2}(p+q+1) = k,$$

as desired. □

Note that it is not too difficult to extend the conclusion of Lemma 2.3.5 to an interval containing p/q as in [Bertozzi et al. 2021, Lemma 92], but we do not need this here. We conclude this subsection with Figure 6, which illustrates the constraint a single obstruction at a single z-value imposes on the embedding capacity function.

2.4. ***Almost toric fibrations.*** Symplectic embeddings provide a useful counterpoint to the obstructions described in Sections 2.2–2.3. We will use combinatorial techniques developed in the theory of *almost toric fibrations* (*ATFs*) to establish the existence of embeddings. Introduced in [Symington 2003] and developed further in [Evans 2023; Leung and Symington 2010], an ATF is a completely

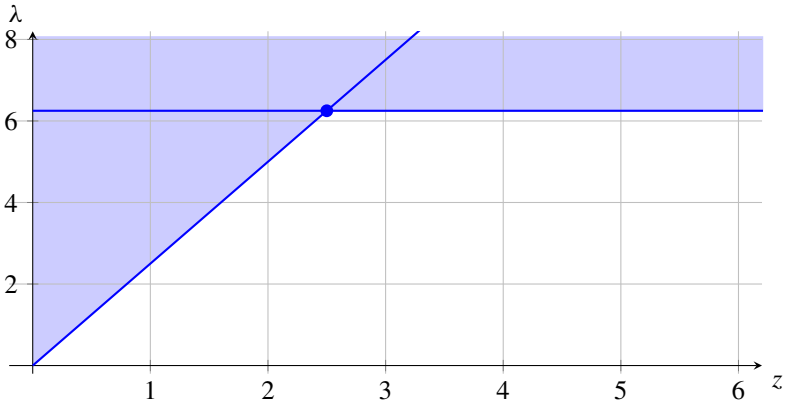

Figure 6. The figure depicts the effect of an obstruction providing a lower bound for c_X at the indicated blue point. The ellipsoid embedding function c_X must lie in the blue shaded region by Proposition 1.0.1 (ii), (iii).

integrable system on a compact symplectic four-manifold with elliptic and focus-focus singularities. This framework provides a map from the manifold M to $\mathbb{R}^2$ whose image is called the *base diagram*. There are combinatorial operations called *nodal trades*, *nodal slides*, and *mutation* on the base diagram that correspond to symplectomorphisms of the corresponding manifolds. These allow us to discover embeddings of ellipsoids into the manifold M by identifying appropriate triangles inside the variously manipulated base diagrams. We may then use Proposition 2.1.4 to deduce that the convex toric domain X also has the same ellipsoid embeddings.

In order to study the polydisk $P(1, \beta)$ with ATFs, we first find a compact manifold that has an ATF with base diagram the $1 \times b$ rectangle. The manifold $M_\beta = \mathbb{C}P^1_1 \times \mathbb{C}P^1_\beta$, a product of two copies of projective space, the first with size 1 and the second with size β, is equipped with a toric T^2 action by rotation in each factor. This has moment map image the Delzant polygon which is the $1 \times \beta$ rectangle. This is our starting point for manipulations using ATF tools. These tools will change the map $M_\beta \to \mathbb{R}^2$ and its image, but not the manifold M_β itself.

The first step is to apply a *nodal trade* at each of the three vertices X, Y, and V which are not at the origin in $\mathbb{R}^2$. Geometrically, in M_β, this means excising the neighborhood of the fixed point corresponding to a vertex and then gluing in a local model of a focus-focus singularity. At the level of the base diagram, this corresponds to adding a ray with a marked point emanating from the *anchor* vertex P. Above the marked point on the ray, there is a pinched torus. The pinch point is the new focus-focus singularity for the updated map $M_\beta \to \mathbb{R}^2$. If we let $\vec{E}$ and $\vec{F}$ denote the primitive vectors (in $\mathbb{Z}^2$) pointing along the edges emanating from P, then

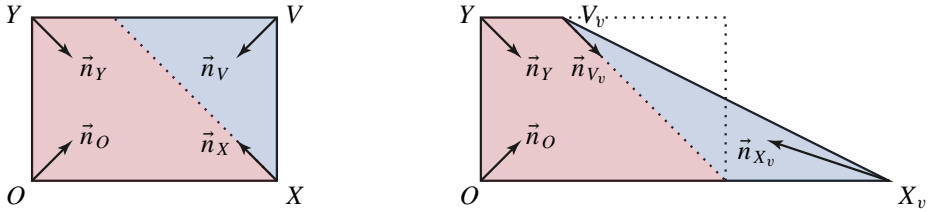

Figure 7. We apply a mutation about the vertex V in the figure on the left to obtain the figure on the right. The mutation fixes the red region and applies an affine linear transformation encoded in a matrix M to the blue region. The effect on the vertices and is indicated. The nodal rays in the figure on the right that differ from those on the left are given by $\vec{n}_{V_v} = -\vec{n}_X$ and $\vec{n}_{X_v} = M \cdot \vec{n}_V$.

the smoothness of M_β guarantees that $\vec{E}$ and $\vec{F}$ form a $\mathbb{Z}$ basis of $\mathbb{Z}^2$. With this notation, then, the nodal ray that we introduce points in the direction $\vec{E} + \vec{F}$. A useful fact, which follows from a straightforward linear algebraic calculation, is that both pairs $(\vec{E}, \vec{E} + \vec{F})$ and $(\vec{E} + \vec{F}, \vec{F})$ are $\mathbb{Z}$ bases of $\mathbb{Z}^2$.

The second operation we can apply to a base diagram is called a *nodal slide*. The local model for a focus-focus singularity has one degree of freedom, corresponding to moving the pinched torus further or closer to the level set above the vertex. In the base diagram, this corresponds to moving the marked point along the nodal ray.

The third operation is *mutation* along a nodal ray of the base diagram. This changes the shape of the diagram. At the level of the function $M_\beta \to \mathbb{R}^2$, if the marked point's location does not move, this corresponds to taking the same function, but choosing a different branch cut to visualize the image of the function.

Combinatorially, the base diagram is divided in two by the line generated by the nodal ray. The mutation operation leaves one piece unchanged (which for us will always be the piece containing the origin) and acts on the other piece by an affine linear transformation that

- fixes the anchor vertex,
- fixes the nodal ray, and
- aligns the two edges emanating from the anchor vertex.

There is a unique transformation in $\mathrm{ASL}_2(\mathbb{Z})$ that achieves this, as a consequence of the linear algebraic fact about the edge rays and nodal rays noted above. The other changes to the base diagram are the creation of a new (anchor) vertex and nodal ray (the negative of the previous). This is illustrated in Figure 7.

Procedurally, we apply a sequence of mutations with the goal of finding wider and wider triangles inside the mutated base diagram. The impact that one mutation has on triangles that fit inside the base diagram is illustrated in Figure 8.

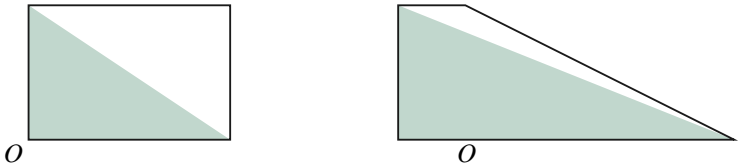

Figure 8. These figures are related by a mutation, as in Figure 7. The fact that the green shaded triangles centered at O have different proportions indicates that we have embeddings of ellipsoids with different eccentricities into the corresponding polydisk.

Remark 2.4.1. When discussing ATF base diagrams and their mutations, we will use the following conventions.

Vertices: We set $O = (0, 0)$, use X and Y to denote the vertices on the x- and y-axes, respectively, and use V to denote the vertex strictly in the positive quadrant.

Nodal rays: The nodal ray of vertex A is labeled $\vec{n}_A$.

Side directions: The primitive integral vector parallel to side AB is denoted $\overrightarrow{AB}$.

Affine lengths: The affine length of the side AB is denoted by $|AB|$.

Mutations: The new vertex at its position (relative to the axes) after a mutation at vertex A has a subscript lowercase a. For example, the vertex on the y-axis after mutation at A is denoted Y_a.

Sequences of mutations: We denote a sequence of mutations by a word in the lowercase letters x, y, v, read from left to right, e.g., v^2yx means "mutate at V twice, then mutate at Y, then mutate at X".

We note that, after a mutation, the nodal rays are transformed in one of three ways: not at all; by taking the negative; or by applying the mutation matrix M. Because our base diagrams are polygons, we will make use of the key identity

$$|OY_a|\overrightarrow{OY}_a + |Y_aV_a|\overrightarrow{Y_aV}_a - |X_aV_a|\overrightarrow{X_aV}_a - |OX_a|\overrightarrow{OX}_a = \begin{pmatrix}0\\0\end{pmatrix}, \qquad (2\text{-}4\text{-}1)$$

derived from the fact that the four sides must close up.

The following result makes precise the relationship between triangles in the base diagram and symplectic embeddings of ellipsoids.

Proposition 2.4.2 [Cristofaro-Gardiner et al. 2020, Proposition 2.35]. *Suppose that a symplectic manifold X is equipped with an almost toric fibration with base diagram Δ_X that consists of a closed region in $\mathbb{R}^2_{\geq 0}$ that is bounded by the axes and a convex (piecewise-linear) curve from $(a, 0)$ to $(0, b)$, for $a, b \in \mathbb{R}^+$. Suppose in addition that there is no nodal ray emanating from $(0, 0)$. Then there exists a symplectic embedding of the ellipsoid $(1 - \varepsilon) \cdot E(a, b)$ into X for any $0 < \varepsilon < 1$.*

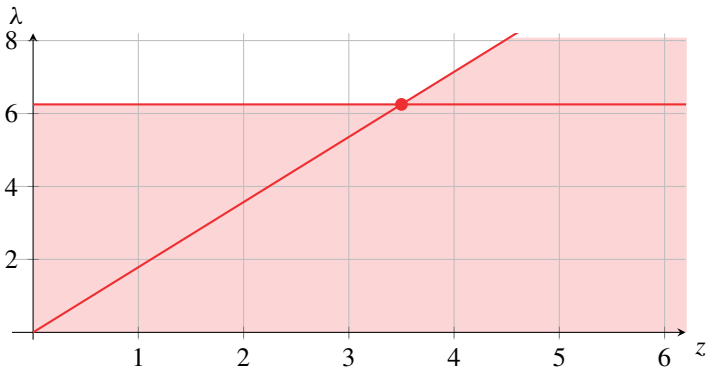

Figure 9. By contrast to Figure 6, an embedding provides an upper bound for c_X at the indicated red point. The function c_X must lie in the red shaded region by Proposition 1.0.1 (ii), (iii).

While the obstructions in Sections 2.2–2.3 give lower bounds on c_X, as indicated in Figure 6, a single embedding forces certain upper bounds on the embedding capacity function. As we will see, the combination of the two can strongly restrict c_X.

2.5. ***Combining obstructions and embeddings.*** Combining the effects in Figures 6 and 9, we see how to prove that the combination of lower bounds provided by obstructions (quasiperfect Diophantine classes or ratios of ECH capacities) with upper bounds provided by an embedding allows us to establish the existence of an infinite staircase. A combination of obstructions and embeddings allows us to nail down the ellipsoid embedding function for some ranges of z-values (indicated by violet segments in Figure 10), and provides bounds on c_X for other ranges of z-values (indicated by violet regions in Figure 10). In this way, one can establish the existence of an infinite staircase without computing the entire function. Or if the embeddings and obstructions are lined up just so, one might just compute the entire function. Note, this is usually only a effective strategy before the accumulation point.

3. Proof of the main theorem

In this section, we prove that the polydisk $P(1, \beta)$ has an infinite staircase accumulating to $\mathrm{acc}(\beta)$, where

$$\beta = \tfrac{1}{12}(6+5\sqrt{30}) \quad \text{and} \quad \mathrm{acc}(\beta) = \tfrac{1}{14}(54+11\sqrt{30}). \tag{3-0-1}$$

The fact that $\mathrm{acc}(\beta)$ satisfies (2-1-1) with $\mathrm{acc}(\beta) = z$ can be verified by hand. Furthermore, set

$$\boldsymbol{E} = (17, 6, 41, 5, 22).$$

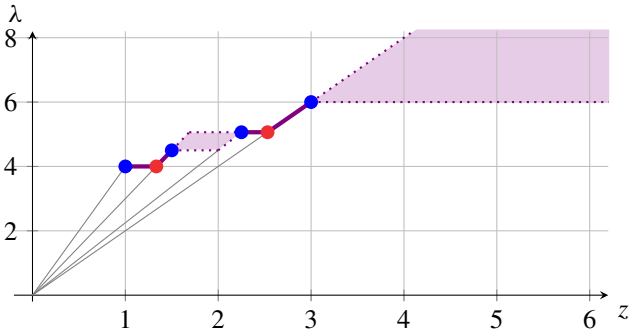

Figure 10. This figure indicates several obstructions at the blue dots and embeddings at the red dots. Combining the bounds forced by these as shown in Figures 6 and 9, we deduce that the ellipsoid embedding function must equal the violet segments and must lie in the violet shaded regions. In particular, it must be constant along the horizontal segment between the blue and red points at the same λ-value; and equal the line when a red point and blue point lie on a line through the origin.

The utility of $\boldsymbol{E}$ is that it is a quasiperfect Diophantine class whose obstruction $\mu_{\boldsymbol{E},\beta}$ equals the function c_β for $z \in \left(\mathrm{acc}(\beta), \frac{41}{5}\right]$. We do not prove this latter claim, but note that on $\left(\mathrm{acc}(\beta), \frac{41}{5}\right]$ we do know — as shown in Figure 6 by setting the blue point equal to $\left(\frac{41}{5}, \mu_{\boldsymbol{E},\beta}\left(\frac{41}{5}\right)\right)$ — that

$$c_\beta(z) \geq z \frac{\mu_{\boldsymbol{E},\beta}\left(\frac{41}{5}\right)}{\frac{41}{5}} = \frac{5z}{17+6\beta}.$$

This is a special case of the analogous [Bertozzi et al. 2021, Proposition 42]. The numerics of $\boldsymbol{E}$ will be crucial for studying c_β.

We next define the obstructions which we will use to prove that c_β has an infinite staircase, following the procedure outlined in Section 2.5.

Definition 3.0.1. We define the *outer class*

$$\boldsymbol{E}_k := t\boldsymbol{E}_{k-1} - \boldsymbol{E}_{k-2} = (d_k, e_k, p_k, q_k, t_k),$$

where $\boldsymbol{E}_0 = (3, 1, 7, 1, 4)$ and $\boldsymbol{E}_1 = (64, 23, 155, 19, 82)$. The recursion constant is $t = 22$ for all k.

Definition 3.0.2. We define the *inner class*

$$\hat{\boldsymbol{E}}_k := t_{k-1}\boldsymbol{E}_k - \boldsymbol{E} = (\hat{d}_k, \hat{e}_k, \hat{p}_k, \hat{q}_k, \hat{t}_k).$$

Note, $\hat{\boldsymbol{E}}_1 = (239, 86, 579, 71, 250)$.

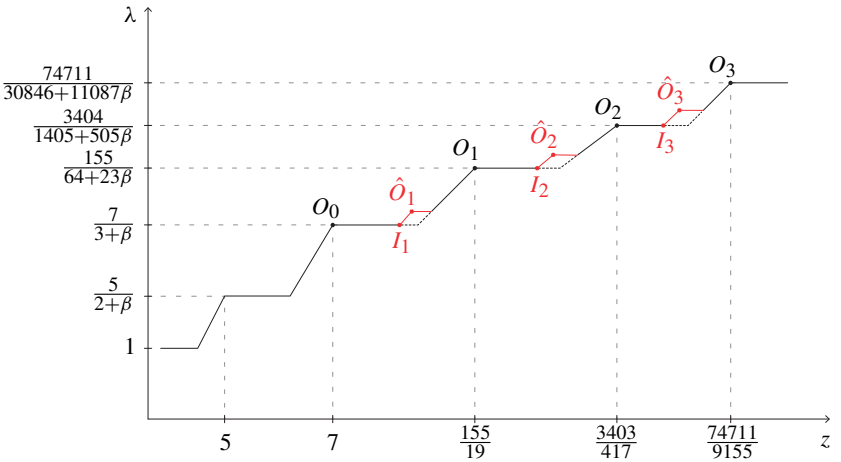

Figure 11. Here is the arrangement of the first several outer and inner corners of c_β. The black outer corners, labeled O_k, arise from the outer $\boldsymbol{E}_k$ classes, and their coordinates are given in Proposition 3.0.4 (i). The red outer corners, labeled $\hat{O}_k$, arise from the inner $\hat{\boldsymbol{E}}_k$ classes, and their coordinates are given in Proposition 3.0.4 (ii). Because c_β does not equal the obstruction $\mu_{\boldsymbol{E}_k,\beta}$ from the outer $\boldsymbol{E}_k$ classes near the intersection of $\mu_{\boldsymbol{E}_k,\beta}$ and $\mu_{\boldsymbol{E}_{k+1},\beta}$, these obstructions are indicated by dashed black lines where the obstructions $\mu_{\hat{\boldsymbol{E}}_{k+1},\beta}$ are larger.

Remark 3.0.3. In the sense of [Magill et al. 2024], the inner class $\hat{\boldsymbol{E}}_k$ is the x-mutation of the triple $(\boldsymbol{E}_{k-1}, \boldsymbol{E}_k, \boldsymbol{E})$. We discovered the $\hat{\boldsymbol{E}}_k$ classes after Mike Usher pointed out the relationship between the $\hat{A}$ classes in [Usher 2019] and x-mutation, see Section 4.2.

The outer corners of the $\boldsymbol{E}_k$ and $\hat{\boldsymbol{E}}_k$ classes alternate in the sense that

$$\cdots < \frac{p_{k-1}}{q_{k-1}} < \frac{\hat{p}_k}{\hat{q}_k} < \frac{p_k}{q_k} < \cdots,$$

while the values their obstructions take at these z-values also alternate. See Lemma 3.1.4, which is illustrated by Figure 11.

In Section 3.1, we will prove the following proposition computing the value of c_β at the outer corners of its infinite staircase.

Proposition 3.0.4. *We establish the following lower bounds on c_β.*

(i) *The outer classes $\boldsymbol{E}_k$ determine the lower bounds*

$$c_\beta\left(\frac{p_k}{q_k}\right) \geq \frac{p_k}{d_k + e_k\beta}.$$

(ii) *The inner classes $\hat{\boldsymbol{E}}_k$ determine the lower bounds*

$$c_\beta\left(\frac{\hat{p}_k}{\hat{q}_k}\right) \geq \frac{\hat{p}_k}{\hat{d}_k + \hat{e}_k\beta}.$$

We will also prove that the claimed outer corners $z = p_k/q_k$ have four-periodic continued fractions, which, upon proving Theorem 1.1.1 part (i), proves part (ii).

Our final definition in this section provides notation for the intersections between the obstructions from $\boldsymbol{E}_k$ and $\hat{\boldsymbol{E}}_k$.

Definition 3.0.5. We set the following notation.

- We denote the points discussed in Proposition 3.0.4 by

$$O_k = \left(\frac{p_k}{q_k}, \frac{p_k}{d_k + e_k\beta}\right) \quad \text{and} \quad \hat{O}_k = \left(\frac{\hat{p}_k}{\hat{q}_k}, \frac{\hat{p}_k}{\hat{d}_k + \hat{e}_k\beta}\right).$$

- We extend the lower bounds at O_k and $\hat{O}_k$ by horizontal lines and lines through the origin, using Proposition 1.0.1 (ii), (iii), as illustrated in Figure 6.
  - Denote by $I_{k+1} = (z^{\text{in}}_{k+1}, \lambda^{\text{in}}_{k+1})$ the intersection between the horizontal line through O_k and the line through the origin and $\hat{O}_{k+1}$.
  - Denote by $\hat{I}_{k+1} = (\hat{z}^{\text{in}}_{k+1}, \hat{\lambda}^{\text{in}}_{k+1})$ the intersection between the horizontal line through $\hat{O}_{k+1}$ and the line through the origin and O_{k+1}.

In Section 3.2, we will use ATFs to construct embeddings computing the value of c_β at the points I_k, proving that they are inner corners. Specifically, we will show:

Proposition 3.0.6. *At the intersections of the obstructions from $\boldsymbol{E}_k$ and $\hat{\boldsymbol{E}}_{k+1}$, we have the upper bound*

$$c_\beta(z^{\text{in}}_{k+1}) \leq \lambda^{\text{in}}_{k+1}.$$

Next we state our conjecture which would, if proven, fully compute c_β on $[1, \text{acc}(\beta)]$. See Remark 3.2.15 for a discussion of the complications which arise in its potential proof.

Conjecture 3.0.7. *At the intersections of the obstructions from $\hat{\boldsymbol{E}}_{k+1}$ and $\boldsymbol{E}_{k+1}$, we have the upper bound*

$$c_\beta(\hat{z}^{\text{in}}_{k+1}) \leq \hat{\lambda}^{\text{in}}_{k+1}.$$

Next we compute the coordinates of I_{k+1} and $\hat{I}_{k+1}$.

Lemma 3.0.8. (i) *We have*

$$(z^{\text{in}}_{k+1}, \lambda^{\text{in}}_{k+1}) = \left(\frac{p_k(\hat{d}_{k+1} + \hat{e}_{k+1}\beta)}{\hat{q}_{k+1}(d_k + e_k\beta)}, \frac{p_k}{d_k + e_k\beta}\right).$$

(ii) *We have*

$$(\hat{z}^{\text{in}}_{k+1}, \hat{\lambda}^{\text{in}}_{k+1}) = \left(\frac{\hat{p}_{k+1}(d_{k+1} + e_{k+1}\beta)}{q_{k+1}(\hat{d}_{k+1} + \hat{e}_{k+1}\beta)}, \frac{\hat{p}_{k+1}}{\hat{d}_{k+1} + \hat{e}_{k+1}\beta}\right).$$

Proof. The values of $\lambda_{k+1}^{\text{in}}$ and $\hat{\lambda}_{k+1}^{\text{in}}$ are immediate because they are the λ-values of the obstructions from $\boldsymbol{E}_k$ and $\hat{\boldsymbol{E}}_{k+1}$, respectively.

To compute z_{k+1}^{in}, we solve

$$\frac{p_k}{d_k + e_k\beta} = \frac{\hat{p}_{k+1}/(\hat{d}_{k+1} + \hat{e}_{k+1}\beta)}{\hat{p}_{k+1}/\hat{q}_{k+1}} z_{k+1}^{\text{in}}$$

for z_{k+1}^{in}, while to compute $\hat{z}_{k+1}^{\text{in}}$, we solve

$$\frac{\hat{p}_{k+1}}{\hat{d}_{k+1} + \hat{e}_{k+1}\beta} = \frac{p_{k+1}/(d_{k+1} + e_{k+1}\beta)}{p_{k+1}/q_{k+1}} \hat{z}_{k+1}^{\text{in}}$$

for $\hat{z}_{k+1}^{\text{in}}$. □

Proof of Theorem 1.1.1 (i). The lower bounds in Proposition 3.0.4 (i) and (ii) combined with the upper bound in Proposition 3.0.6 prove, by Lemma 3.0.8 (i), that c_β has infinitely many nonsmooth points at the inner corners between the obstructions from $\boldsymbol{E}_k$ and $\hat{\boldsymbol{E}}_{k+1}$, as indicated in Figure 10. (These inner corners are labeled I_{k+1} in Figure 11.) Note that, to conclude that $c_\beta(p_k/q_k) = c_\beta(z_{k+1}^{\text{in}})$, we use the fact that c_β is increasing, which requires Lemma 3.1.4 to know that

$$\frac{p_k}{q_k} \le z_{k+1}^{\text{in}} \le \frac{\hat{p}_{k+1}}{\hat{q}_{k+1}}.$$ □

Remark 3.0.9. Note that if we could show Conjecture 3.0.7, then, by Lemma 3.0.8 and similar reasoning to the proof of Theorem 1.1.1 (i), we would be able to compute the entire function c_β between the center 7 of $\boldsymbol{E}_0$ and $\text{acc}(\beta) = \frac{1}{14}(54 + 11\sqrt{30})$. (It is very little extra work to compute c_β on $[1, 7]$, since it requires identifying only two outer and two inner corners.)

3.1. ***Outer corners.*** To prove Proposition 3.0.4, it suffices by (2-2-3) to show that the recursively defined families $\boldsymbol{E}_k$ and $\hat{\boldsymbol{E}}_k$ satisfy the Diophantine equations (2-2-1).

For our proof, we use the ideas developed in [Magill and McDuff 2023, Section 2.2] to think of a quasiperfect class as a integral point (p, q, t) on a quadratic surface X, where $t = \sqrt{p^2 + q^2 - 6pq + 8}$. In particular, as noted in Lemma 2.2.5, a tuple $(d, e; p, q, t)$ will satisfy the Diophantine equations if, given an integral tuple $(p, q, t) \in X$, we define[5] d and e by

$$4d = p + q + t \quad \text{and} \quad 4e = p + q - t.$$

We then use the result [Magill and McDuff 2023, Lemma 3.1.2] which allows us to see that we can produce new tuples $(p, q, t) \in X$ via recursion assuming certain

[5]Note, as defined in this way, (d, e) might not be integers for all integral choices of (p, q, t). Thus, not all points on X correspond to quasiperfect classes.

compatibility conditions hold. Let

$$A := \begin{pmatrix} -1 & 3 & 0 \\ 3 & -1 & 0 \\ 0 & 0 & 1 \end{pmatrix}, \quad \boldsymbol{x} := \begin{pmatrix} p \\ q \\ t \end{pmatrix}.$$

Then the surface X is given by $\{\boldsymbol{x}^T A\boldsymbol{x} = 8\}$, as $\boldsymbol{x}^T A\boldsymbol{x} = 6pq - p^2 - q^2 + t^2$.

We can now state the lemma.

Lemma 3.1.1 [Magill and McDuff 2023, Lemma 3.1.2]. *Suppose that $\boldsymbol{x}_0$ and $\boldsymbol{x}_1$ are integral vectors that satisfy the following conditions for some integer $\nu > 0$:*

$$\boldsymbol{x}_i^T A\boldsymbol{x}_i = 8, \qquad i = 0, 1, \tag{3-1-1}$$

$$\boldsymbol{x}_1^T A\boldsymbol{x}_0 = 4\nu. \tag{3-1-2}$$

Then, the vectors $\boldsymbol{x}_2 := \nu\boldsymbol{x}_1 - \boldsymbol{x}_0, \boldsymbol{x}_1$ also satisfy these conditions for the given ν.

We can then restate [Magill and McDuff 2023, Corollary 3.1.1] for our purposes.

Corollary 3.1.2. *Any two integral triples $\boldsymbol{x}_i = (p_i, q_i, t_i)$, $i = 0, 1$, that satisfy (3-1-1) and (3-1-2) for a given ν can be extended to a sequence*

$$\boldsymbol{x}_i := \nu\boldsymbol{x}_{i-1} - \boldsymbol{x}_{i-2}, \quad i \geq 0,$$

and each successive adjacent pair satisfies these conditions. Further, the corresponding quantities

$$d_i = \tfrac{1}{4}(p + q + t), \quad e_i = \tfrac{1}{4}(p + q - t)$$

also satisfy this recursion and hence are integers, provided that they are integers for $i = 0, 1$.

We now proceed to proving Proposition 3.0.4 giving the bounds for the outer corners at $z_k = p_k/q_k$ and $\hat{z}_k = \hat{p}_k/\hat{q}_k$.

Proof of Proposition 3.0.4. To prove (i) and (ii), we must check that the classes $\boldsymbol{E}_k = t\boldsymbol{E}_{k-1} - \boldsymbol{E}_{k-2}$ and $\hat{\boldsymbol{E}}_k = t_{k-1}\boldsymbol{E}_k - \boldsymbol{E}$ are Diophantine classes. By Corollary 3.1.2 and Lemma 2.2.5, it is enough to verify the following:

- $\boldsymbol{E}_k$ and $\boldsymbol{E}$ satisfy (3-1-1).
- $\boldsymbol{E}_0 = (3, 1, 7, 1, 4)$ and $\boldsymbol{E}_1 = (64, 23, 155, 19, 82)$ satisfy (3-1-2) for $\nu = t = 22$.
- $\hat{\boldsymbol{E}}_k$ and $\boldsymbol{E} = (17, 6, 41, 5, 22)$ satisfy (3-1-2) for $\nu = t_{k-1}$.

By Corollary 3.1.2, (3-1-1) will hold for $\boldsymbol{E}_k$ if it holds for $\boldsymbol{E}_0$ and $\boldsymbol{E}_1$. Thus, we must check this for $\boldsymbol{E}_0$, $\boldsymbol{E}_1$, and $\boldsymbol{E}$. We have

$$\begin{aligned} \boldsymbol{E}_0: &\ 6(7) - 7^2 - 1^2 + 4^2 = 8, \\ \boldsymbol{E}_1: &\ 6(155)(19) - 155^2 - 19^2 + 82^2 = 8, \\ \boldsymbol{E}: &\ 6(41)(5) - 41^2 - 5^2 + 22^2 = 8. \end{aligned}$$

Now, we check (3-1-2) for $\boldsymbol{E}_0$ and $\boldsymbol{E}_1$ with $\nu = 22$:

$$1(3\cdot 155 - 19) + 7(3\cdot 19 - 155) + 82\cdot 4 = 4\cdot 22.$$

To check (3-1-2) for the pair $\boldsymbol{E}_k$ and $\boldsymbol{E}$ with $\nu = t_{k-1}$, this involves verifying

$$5(3p_k - q_k) + 41(3q_k - p_k) + 22t_k = 4t_{k-1}.$$

As this is a linear equation, we can verify it holds by induction by checking for $k = 1, 2$. This is an easy computation.

Thus, $\boldsymbol{E}_k$ and $\hat{\boldsymbol{E}}_k$ are quasiperfect Diophantine classes, and (i) and (ii) follow by (2-2-2) and (2-2-3). □

Remark 3.1.3. As in the proof of Lemma 2.3.5, if $\boldsymbol{E} = (d, e, p, q, t)$ and $\Lambda_{\boldsymbol{E}}$ represents the convex lattice path with corners the origin, $(0, e)$, (d, e), and $(d, 0)$, then with

$$k = \mathcal{L}(\Lambda_{\boldsymbol{E}}) = \tfrac{1}{2}(p+1)(q+1) - 1 = (d+1)(e+1) - 1,$$

we have

$$c_\beta\left(\frac{p}{q}\right) \geq \frac{N_k(1, p/q)}{\ell_{\Omega_\beta}(\Lambda_{\boldsymbol{E}})} = \frac{p}{d + e\beta}.$$

Thus to prove Proposition 3.0.4 (i) and (ii), it would also suffice to simply identify the lattice paths $\Lambda_{\boldsymbol{E}_k}$ and $\Lambda_{\hat{\boldsymbol{E}}_k}$.

Next we prove that the centers of the quasiperfect Diophantine classes $\boldsymbol{E}_k$ and $\hat{\boldsymbol{E}}_k$ are arranged as depicted in Figure 11 on page 47.

Lemma 3.1.4. (i) *The centers of the classes $\boldsymbol{E}_k$ and $\hat{\boldsymbol{E}}_k$ alternate*:

$$\cdots < \frac{p_k}{q_k} < \frac{\hat{p}_{k+1}}{\hat{q}_{k+1}} < \frac{p_{k+1}}{q_{k+1}} < \cdots.$$

(ii) *The obstructions from the classes $\boldsymbol{E}_k$ and $\hat{\boldsymbol{E}}_k$ alternate*:

$$\cdots < \frac{p_k}{d_k + e_k\beta} < \frac{\hat{p}_{k+1}}{\hat{d}_{k+1} + \hat{e}_{k+1}\beta} < \frac{p_{k+1}}{d_{k+1} + e_{k+1}\beta} < \cdots.$$

Proof. Our goal is to show

$$\frac{p_k}{q_k} < \frac{\hat{p}_{k+1}}{\hat{q}_{k+1}} < \frac{p_{k+1}}{q_{k+1}}. \tag{3-1-3}$$

The first inequality in (3-1-3) is equivalent to

$$\begin{aligned} p_k\hat{q}_{k+1} &< q_k\hat{p}_{k+1}, \\ p_k(t_k q_{k+1} - 5) &< q_k(t_k p_{k+1} - 41), \\ t_k p_k q_{k+1} - 5p_k &< t_k p_{k+1} q_k - 41q_k, \end{aligned}$$

which follows if we can show that

$$\frac{p_k}{q_k} < \frac{p_{k+1}}{q_{k+1}} \quad \text{and} \quad \frac{p_k}{q_k} < \tfrac{41}{5}. \tag{3-1-4}$$

Similarly, the second inequality in (3-1-3) is equivalent to

$$\begin{aligned} \hat{p}_{k+1}q_{k+1} &< p_{k+1}\hat{q}_{k+1}, \\ (t_k p_{k+1} - 41)q_{k+1} &< p_{k+1}(t_k q_{k+1} - 5), \\ t_k p_{k+1}q_{k+1} - 41q_{k+1} &< t_k p_{k+1}q_{k+1} - 5p_{k+1}, \end{aligned}$$

which follows from the second inequality in (3-1-4).

The first inequality in (3-1-4) is

$$p_k(22q_k - q_{k-1}) < q_k(22p_k - p_{k-1}) \quad \Longleftrightarrow \quad p_{k-1}q_k < p_k q_{k-1},$$

and thus follows by induction and the base case $k = 1$:

$$\frac{p_0}{q_0} = 7, \quad \frac{p_1}{q_1} = \tfrac{155}{19} \approx 8.158.$$

The second inequality in (3-1-4) is equivalent to a linear inequality in p_k and q_k, which holds because they both satisfy the same recursion and it holds for $k = 0$:

$$5p_0 < 41q_0 \quad \Longleftrightarrow \quad 5 \cdot 7 < 41 \cdot 1.$$

To prove (ii), notice that

$$\hat{d}_{k+1} + \hat{e}_{k+1}\beta = t_k(d_{k+1} + e_{k+1}\beta) + 17 + 6\beta,$$

thus by the same logic as in the proof of (i), all we need to show is

$$\frac{p_k}{d_k + e_k\beta} < \frac{p_{k+1}}{d_{k+1} + e_{k+1}\beta}, \quad \frac{p_k}{d_k + e_k\beta} < \frac{41}{17 + 6\beta}. \tag{3-1-5}$$

The first inequality in (3-1-5) is

$$\begin{aligned} p_k(22d_k - d_{k-1} + 22e_k\beta - e_{k-1}\beta) < (22p_k - p_{k-1})(d_k + e_k\beta) \\ \Longleftrightarrow \quad \frac{p_{k-1}}{d_{k-1} + e_{k-1}\beta} < \frac{p_k}{d_k + e_k\beta}, \end{aligned}$$

which follows by induction and the base case $k = 1$:

$$\frac{7}{3 + \beta} < \frac{155}{64 + 23\beta} \quad \Longleftrightarrow \quad 6\beta < 17,$$

which holds because $6\beta \approx 16.693$.

The second inequality in (3-1-5) is equivalent to a linear inequality in terms satisfying the same recursion, thus we simply need to check it for $k = 0$:

$$\frac{7}{3 + \beta} \approx 1.211 < 1.217 \approx \frac{41}{17 + 6\beta}. \qquad \square$$

Proof of Theorem 1.1.1 (ii) assuming (i). As above, let $\{p_k/q_k\}$ be the sequence of rational numbers described by the recursion with seeds $p_0 = 7,\ q_0 = 1$ and $p_1 = 155,\ q_1 = 19$ and relation

$$p_k = 22p_{k-1} - p_{k-2}, \quad q_k = 22q_{k-1} - q_{k-2}$$

for $k \geq 2$. We prove that this sequence coincides with the sequence of continued fractions of the form

$$\left[8, 6, 4, 2, \frac{u_{k-2}}{v_{k-2}}\right] =: \frac{u_k}{v_k}$$

for all $k \geq 2$. Here, we assume that the seeds of both recursions are equal, so $u_j = p_j$ and $v_j = q_j$ for $j = 0, 1$.

To prove this equality, we use the following standard result of number theory, which is explained in Chapter 2.1 of [Hatcher 2022].

Lemma 3.1.5. *Let the continued fraction for a real number α be $[a_0, a_1, a_2, \dots]$. If $\{r_n/s_n\}$ denotes the sequence of convergents of α obtained by truncating this continued fraction expansion, then, for any real number z,*

$$[a_0, a_1, a_2, \dots, a_n, z] = \frac{zr_n + r_{n-1}}{zs_n + s_{n-1}}.$$

Furthermore, $r_{n+1}s_n - r_n s_{n+1} = (-1)^n$ for all $n \geq 0$.

The number $\alpha = \frac{1}{14}(54 + 11\sqrt{30}) = \mathrm{acc}(\beta)$ has the 4-periodic continued fraction

$$\alpha = [\{8, 6, 4, 2\}^\infty].$$

The numerators and denominators of the second and third convergents of this continued fraction are $r_2 = 204,\ s_2 = 25,\ r_3 = 457$, and $s_3 = 56$. Lemma 3.1.5 combined with our recurrence relation yields

$$\frac{u_k}{v_k} = \left[8, 6, 4, 2, \frac{u_{k-2}}{v_{k-2}}\right] = \frac{r_3u_{k-2} + r_2v_{k-2}}{s_3u_{k-2} + s_2v_{k-2}}$$

for all $k \geq 2$. This can also be written using matrix notation:

$$\begin{pmatrix} u_k \\ v_k \end{pmatrix} = \begin{pmatrix} r_3 & r_2 \\ s_3 & s_2 \end{pmatrix} \begin{pmatrix} u_{k-2} \\ v_{k-2} \end{pmatrix}. \tag{3-1-6}$$

We assume $x_j = 22x_{j-1} - x_{j-2}$ for $j < k$ and $x_j = u_j, v_j$. By (3-1-6), we have

$$u_k = 22u_{k-1} - u_{k-2},$$
$$r_3u_{k-2} + r_2v_{k-2} = 22(r_3u_{k-3} + r_2v_{k-3}) - (r_3u_{k-4} + r_2v_{k-4}),$$

which follows from the inductive hypothesis. Similarly, we may obtain $v_k = 22v_{k-1} - v_{k-2}$ from $v_k = s_3u_{k-2} + s_2v_{k-2}$.

Thus, the sequence of rational numbers $\{u_k/v_k\}$ is determined by the same seeds and the same recurrence relation as the sequence $\{p_k/q_k\}$, as claimed. □

We have also shown the following.

Corollary 3.1.6. *The limit of the outer corners is*

$$\lim_{k\to\infty} \frac{p_k}{q_k} = \operatorname{acc}(\beta).$$

Proof. The continued fractions of the ratios p_k/q_k converge to the continued fraction of $\alpha = [\{8, 6, 4, 2\}^\infty] = \operatorname{acc}(\beta)$. □

Corollary 3.1.6 may also be proved by solving the recursion in Definition 3.0.1, see [Bertozzi et al. 2021, Proposition 49], however we do not do this here.

3.2. ***Inner corners.*** We describe a family of mutations whose existence proves Proposition 3.0.6 and explains the reasoning behind Conjecture 3.0.7. Throughout we will freely use the conventions discussed in Remark 2.4.1.

The following definition is a version of [Magill et al. 2024, Definition 2.1.1]. It describes algebraic relations between various classes, which later will be helpful in showing various identities hold that arise in the ATF proofs.

Definition 3.2.1. Two classes $\boldsymbol{E} := (d, e, p, q, t)$ and $\boldsymbol{E}' := (d', e', p', q', t')$ that are quasiperfect are said to be *adjacent* if, after renaming so that $p/q < p'/q'$ (if necessary), the following relation holds:

$$(p+q)(p'+q') - tt' = 8pq'.$$

Further, they are called t''*-compatible* if

$$tt' - 4t'' = pp' - 3(pq' + qp') + qq', \qquad \text{i.e., } \boldsymbol{x}^T A \boldsymbol{x}' = 4t''.$$

The following lemma about t-compatibility and adjacency is from [Magill et al. 2024, Lemma 2.1.2]. It proves how compatibility and adjacency hold throughout a recursive sequence. Note that this proof did not use the (d, m) coordinates used in [Magill et al. 2024] and just uses the (p, q, t) coordinates, and thus, the lemma holds for our classes here.

Lemma 3.2.2. (i) *Suppose that the points* $\boldsymbol{x}_0 := (p_0, q_0, t_0)$ *and* $\boldsymbol{x}_1 := (p_1, q_1, t_1)$ *are* t*-compatible for some* $t \geq 3$ *and have, coordinate by coordinate,* $\boldsymbol{x}_0 < \boldsymbol{x}_1$*. Then* $\boldsymbol{x}_2 := t\boldsymbol{x}_1 - \boldsymbol{x}_0 \geq 0$*. Also,* $\boldsymbol{x}_1 < \boldsymbol{x}_2$*, and the pair* $\boldsymbol{x}_1, \boldsymbol{x}_2$ *is* t*-compatible. Further, if* $\boldsymbol{x}_0, \boldsymbol{x}_1$ *are adjacent, so are* $\boldsymbol{x}_1, \boldsymbol{x}_2$*. Thus, if* $\boldsymbol{E}_0, \boldsymbol{E}_1$ *satisfy* $p_0 < p_1$*,* $q_0 < q_1$*,* $t_0 < t_1$ *and are adjacent and* t*-compatible, then so are the components of all successive pairs in the sequence obtained from* $\boldsymbol{E}_0, \boldsymbol{E}_1$ *by* t*-recursion.*

(ii) *If* $\boldsymbol{E}$ *and* $\boldsymbol{E}'$ *are adjacent, then they are* t''*-compatible exactly if*

$$|p'q - pq'| = t''.$$

Recall that $\boldsymbol{E} = (d, e, p, q, t) = (17, 6, 41, 5, 22)$. The following lemma comes from [Magill 2024, Lemma 4.6].

Lemma 3.2.3. *For the classes $\boldsymbol{E}_\lambda$, $\boldsymbol{E}_\mu$, $\boldsymbol{E}_\rho$, where $(\boldsymbol{E}_\lambda, \boldsymbol{E}_\mu, \boldsymbol{E}_\rho) := (\boldsymbol{E}_k, \boldsymbol{E}_{k+1}, \boldsymbol{E})$ or $(\boldsymbol{E}_\lambda, \boldsymbol{E}_\mu, \boldsymbol{E}_\rho) := (\boldsymbol{E}_k, \hat{\boldsymbol{E}}_{k+1}, \boldsymbol{E}_{k+1})$, the following identities hold*:

(i) $p_\lambda + q_\lambda = q_\mu t_\rho - q_\rho, t_\mu$ *and* $7p_\lambda - q_\lambda = p_\mu t_\rho - t_\mu p_\rho$,

(ii) $p_\rho + q_\rho = p_\mu t_\lambda - p_\lambda t_\mu$ *and* $p_\rho - 7q_\rho = q_\lambda t_\mu - q_\mu t_\lambda$,

(iii) $p_\mu + q_\mu = q_\rho t_\lambda + p_\lambda t_\rho$, $7p_\mu - q_\mu = 6p_\lambda t_\rho + p_\rho t_\lambda - q_\lambda t_\rho$, *and* $7q_\mu - p_\mu = 6q_\rho t_\lambda + q_\lambda t_\rho - p_\rho t_\lambda$,

(iv) $p_\lambda(p_\rho - 6q_\rho) + q_\lambda q_\rho = t_\mu$,

(v) $q_\lambda t_\lambda + q_\rho t_\rho + q_\mu t_\mu = q_\mu t_\lambda t_\rho$,

(vi) $t_\lambda \begin{pmatrix} 1 + p_\mu q_\mu - 6q_\mu^2 \\ q_\mu^2 \end{pmatrix} = q_{x\mu} \begin{pmatrix} p_\mu - 6q_\mu \\ q_\mu \end{pmatrix} + q_\mu \begin{pmatrix} p_\rho - 6q_\rho \\ q_\rho \end{pmatrix}$,

(vii) $-t_\rho \begin{pmatrix} -q_\mu^2 \\ q_\mu p_\mu - 1 \end{pmatrix} = q_{y\mu} \begin{pmatrix} q_\mu \\ -p_\mu \end{pmatrix} + q_\mu \begin{pmatrix} q_\lambda \\ -p_\lambda \end{pmatrix}$.

Proof. These identities are a reformulation of the recursion compatibility and adjacency equations proven in [Magill 2024, Lemma 4.6] using the facts that

- $\boldsymbol{E}_\lambda$ and $\boldsymbol{E}_\mu$ are t_ρ-compatible and adjacent,
- $\boldsymbol{E}_\rho$ and $\boldsymbol{E}_\mu$ are t_λ-compatible and adjacent,

which can be proved for the triple $(\boldsymbol{E}_k, \boldsymbol{E}_{k+1}, \boldsymbol{E})$ by induction using Lemma 3.2.2 and for the triple $(\boldsymbol{E}_k, \hat{\boldsymbol{E}}_{k+1}, \boldsymbol{E}_{k+1})$ using [Magill et al. 2024, Proposition 2.1.9]. Note that in the proof of this proposition, the $(d; m)$ coordinates used in [Magill et al. 2024] are not needed, and only the properties of (p, q, t) were needed which are the same coordinates we are using here. □

The first sequence of mutations we consider is v^2yxy^k. We found this sequence by adapting an analogous case found by Magill in [2024, Proposition 3.9].[6] We show in Proposition 3.2.10 that this sequence gives embeddings $(1-\varepsilon)\cdot E(1, z_k) \overset{s}{\hookrightarrow} P(\mathrm{vol}(\beta), \mathrm{vol}(\beta)\beta)$[7] for a sequence z_k such that $\lim_{k\to\infty} z_k = \mathrm{acc}(\beta)$. Each of the points $(z_k, \mathrm{vol}(\beta))$ lie strictly above the embedding function.

Then, for each k, we will perform several additional mutations that provide embeddings $(1-\varepsilon)\cdot E(1, z) \overset{s}{\hookrightarrow} P(\lambda, \lambda\beta)$ where (z, λ) does lie on the graph of the embedding function: specifically, at the inner corners between the obstructions from $\boldsymbol{E}_k$ and $\hat{\boldsymbol{E}}_{k+1}$, proving Proposition 3.0.6.

The effects of the successive mutations in the sequence v^2y^2 are illustrated in Figure 12.

[6] In [Magill 2024], the mutation sequences are instead written from right to left.

[7] Recall that $\mathrm{vol}(\beta) = \mathrm{vol}_\beta(\mathrm{acc}(\beta))$.

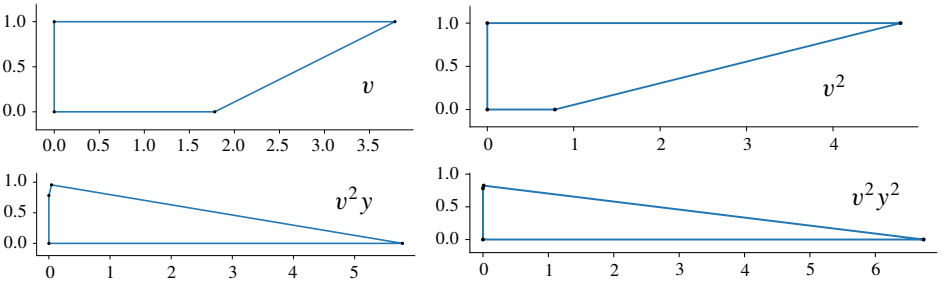

Figure 12. An illustrative example of the mutation sequence v^2y^2, where each figure represents the polygon Ω_β after one step of mutation. The images on the bottom have their axes reflected: the correct figures are the ones displayed with z and λ switched. Already it is clear that more mutations by y would cut the edge XV shorter and shorter. We do not include the mutation by x here, even though the actual sequence considered is v^2yxy, because its effect would be very difficult to see at this scale.

We will frequently use the following simplification of $\mathrm{vol}(\beta)$.

Lemma 3.2.4. *We have the relation*

$$\frac{1}{\mathrm{vol}(\beta)} = -1 + \tfrac{1}{3}\sqrt{30} = \tfrac{1}{5}(4\beta - 7).$$

Proof. Following the method of proof of [Magill and McDuff 2023, Lemma 2.2.7] and replacing $3-b$ with the affine perimeter in our case, which is $2+2\beta$, for any value of β, we have

$$\mathrm{vol}(\beta) = \frac{1+\mathrm{acc}(\beta)}{2+2\beta}.$$

With $\beta = \frac{1}{12}(6+5\sqrt{30})$ and $\mathrm{acc}(\beta) = \frac{1}{14}(54+11\sqrt{30})$, we simplify

$$\frac{1}{\mathrm{vol}(\beta)} = \frac{2+2\cdot\frac{1}{12}(6+5\sqrt{30})}{1+\frac{1}{14}(54+11\sqrt{30})} = -1+\tfrac{1}{3}\sqrt{30}.$$

This proves the first equality. The second is a simple computation. □

Remark 3.2.5. The conclusion of Lemma 3.2.4 is similar to Lemma 5.1 (iii) in [Magill 2024], where we find that in the case of the Hirzebruch surface, if to the right of the accumulation the function $c_\beta(z)$ is given by a class $\boldsymbol{E} = (d, m, p, q, t)$, then

$$\mathrm{vol}(b) = \frac{q}{(m-q)b - (d-3q)},$$

where $\mathrm{vol}(b) = \mathrm{vol}_b(\mathrm{acc}_H(b))$, noting that the volume obstruction $\mathrm{vol}_b(z)$ has the formula $\sqrt{z/(1-b^2)}$ when the target is H_b. In our case, with $\boldsymbol{E} = (17, 6, 41, 5, 22)$, $\beta = \frac{1}{12}(6+5\sqrt{30})$, and our definition of vol, we have

$$\mathrm{vol}(\beta) = \frac{5}{4\beta - 7} = \frac{q}{(2q-e)\beta + (2q-d)}. \tag{3-2-1}$$

We compute the result of the first four mutations, illustrated in Figure 12.

Lemma 3.2.6. *After performing the sequence of mutations v^2yx to the diagram Ω_β, the nodal rays are*

$$\vec{n}_Y = \begin{pmatrix} 1 \\ -7 \end{pmatrix}, \quad \vec{n}_V = \begin{pmatrix} -3 \\ -1 \end{pmatrix}, \quad \vec{n}_X = \begin{pmatrix} 11 \\ 5 \end{pmatrix},$$

the direction vectors are

$$\overrightarrow{OY} = \begin{pmatrix} 0 \\ 1 \end{pmatrix}, \quad \overrightarrow{OX} = \begin{pmatrix} 1 \\ 0 \end{pmatrix}, \quad \overrightarrow{YV} = \begin{pmatrix} 1 \\ -6 \end{pmatrix}, \quad \overrightarrow{XV} = \begin{pmatrix} 56 \\ 25 \end{pmatrix},$$

and the affine lengths are

$$|OY| = 3+\beta, \quad |OX| = \frac{1}{\mathrm{vol}(\beta)}, \quad |YV| = \tfrac{1}{19}(7+4\beta), \quad |XV| = \tfrac{1}{95}(3-\beta).$$

Proof. The diagram Ω_β has nodal rays

$$\vec{n}_Y = \begin{pmatrix} 1 \\ -1 \end{pmatrix}, \quad \vec{n}_V = \begin{pmatrix} -1 \\ -1 \end{pmatrix}, \quad \vec{n}_X = \begin{pmatrix} -1 \\ 1 \end{pmatrix},$$

direction vectors

$$\overrightarrow{OY} = \overrightarrow{XV} = \begin{pmatrix} 0 \\ 1 \end{pmatrix}, \quad \overrightarrow{OX} = \overrightarrow{YV} = \begin{pmatrix} 1 \\ 0 \end{pmatrix},$$

and affine lengths

$$|OY| = |XV| = 1, \quad |OX| = |YV| = \beta.$$

Step 1: *first mutation at V.* The nodal ray $\vec{n}_V$ hits the side OX at $(\beta-1, 0)$, giving us the affine lengths

$$|OY_v| = |X_vV_v| = 1, \quad |OX_v| = \beta - 1, \quad |Y_vV_v| = \beta + 1.$$

The matrix M for mutation at V must satisfy

$$M\vec{n}_V = \vec{n}_V, \quad M\overrightarrow{VX} = \overrightarrow{YV} \iff M = \begin{pmatrix} 2 & -1 \\ 1 & 0 \end{pmatrix}.$$

Thus the result of a V-mutation has nodal rays

$$\vec{n}_{Y_v} = \vec{n}_Y = \begin{pmatrix} 1 \\ -1 \end{pmatrix}, \quad \vec{n}_{V_v} = M\vec{n}_X = \begin{pmatrix} -3 \\ -1 \end{pmatrix}, \quad \vec{n}_{X_v} = -\vec{n}_V = \begin{pmatrix} 1 \\ 1 \end{pmatrix}.$$

The unchanged direction vectors are

$$\overrightarrow{OY_v} = \begin{pmatrix}0\\1\end{pmatrix}, \quad \overrightarrow{OX_v} = \overrightarrow{Y_vV_v} = \begin{pmatrix}1\\0\end{pmatrix}, \quad \text{and} \quad \overrightarrow{X_vV_v} = M\overrightarrow{OX} = \begin{pmatrix}2\\1\end{pmatrix}.$$

Step 2: *second mutation at V*. We now replace each result A_v of Step 1 with A so that we do not have to stack subscripts. The nodal ray $\vec{n}_V = (-3, -1)$ hits the side OX at $(b+1, 1) + (-3, -1) = (b-2, 0)$, giving us the affine lengths

$$|OY_v| = |X_vV_v| = 1, \quad |OX_v| = \beta - 2, \quad |Y_vV_v| = \beta + 2.$$

The mutation matrix M must satisfy

$$M\vec{n}_V = \vec{n}_V, \quad M\overrightarrow{VX} = \overrightarrow{YV} \iff M = \begin{pmatrix}4 & -9\\1 & -2\end{pmatrix}.$$

Thus the nodal rays are

$$\vec{n}_{Y_v} = \vec{n}_Y = \begin{pmatrix}1\\-1\end{pmatrix}, \quad \vec{n}_{V_v} = M\vec{n}_X = \begin{pmatrix}-5\\-1\end{pmatrix}, \quad \vec{n}_{X_v} = -\vec{n}_V = \begin{pmatrix}3\\1\end{pmatrix}.$$

The unchanged direction vectors are

$$\overrightarrow{OY_v} = \begin{pmatrix}0\\1\end{pmatrix}, \quad \overrightarrow{OX_v} = \overrightarrow{Y_vV_v} = \begin{pmatrix}1\\0\end{pmatrix}, \quad \text{and} \quad \overrightarrow{X_vV_v} = M\overrightarrow{OX} = \begin{pmatrix}4\\1\end{pmatrix}.$$

Step 3: *mutation at Y*. Again, we replace A_v with A. The nodal ray $\vec{n}_Y$ hits the side XV, because its x-intercept is at $(1, 0)$ and $\beta - 2 < 1$. The mutation matrix M must satisfy

$$M\vec{n}_Y = \vec{n}_Y, \quad M\overrightarrow{YV} = \overrightarrow{OY} \iff M = \begin{pmatrix}0 & -1\\1 & 2\end{pmatrix}.$$

Thus the nodal rays are

$$\vec{n}_{Y_y} = M\vec{n}_V = \begin{pmatrix}1\\-7\end{pmatrix}, \quad \vec{n}_{V_y} = -\vec{n}_Y = \begin{pmatrix}-1\\1\end{pmatrix}, \quad \vec{n}_{X_y} = \vec{n}_X = \begin{pmatrix}3\\1\end{pmatrix}.$$

The affine lengths are

$$|OY_y| = |OY| + |YV| = \beta + 3, \quad |OX_y| = |OX| = \beta - 2,$$

and the unchanged direction vectors are

$$\overrightarrow{OY_y} = \begin{pmatrix}0\\1\end{pmatrix}, \quad \overrightarrow{OX_y} = \overrightarrow{OX} = \begin{pmatrix}1\\0\end{pmatrix}, \quad \overrightarrow{X_yV_y} = \overrightarrow{XV_y} = \begin{pmatrix}4\\1\end{pmatrix}.$$

Furthermore,

$$\overrightarrow{Y_yV_y} = M\overrightarrow{VX} = M\begin{pmatrix}-4\\-1\end{pmatrix} = \begin{pmatrix}1\\-6\end{pmatrix}.$$

Finally, we solve (2-4-1) with $a = y$ to obtain

$$|Y_v V_v| = \tfrac{1}{5}(\beta+2), \quad |X_y V_y| = \tfrac{1}{5}(3-\beta);$$

note that $|Y_y V_y| + |X_y V_y| = |XV| = 1$.

Step 4: *mutation at* X. We replace A_y with A. The nodal ray $\vec{n}_X$ hits the side YV because it has positive slope. The mutation matrix M must satisfy

$$M\vec{n}_X = \vec{n}_X, \quad M\overrightarrow{XV} = \overrightarrow{OX} \iff M = \begin{pmatrix} -2 & 9 \\ -1 & 4 \end{pmatrix},$$

thus the nodal rays are

$$\vec{n}_{Y_x} = \vec{n}_Y = \begin{pmatrix} 1 \\ -7 \end{pmatrix}, \quad \vec{n}_{V_x} = -\vec{n}_X = \begin{pmatrix} -3 \\ -1 \end{pmatrix}, \quad \vec{n}_{X_x} = M\vec{n}_V = \begin{pmatrix} 11 \\ 5 \end{pmatrix}.$$

The affine lengths are

$$|OY_x| = |OY| = \beta+3, \quad |OX_x| = |OX| + |XV| = \beta - 2 + \tfrac{1}{5}(3-\beta) = \tfrac{1}{5}(4\beta-7),$$

and the unchanged direction vectors are

$$\overrightarrow{OY_x} = \overrightarrow{OY} = \begin{pmatrix} 0 \\ 1 \end{pmatrix}, \quad \overrightarrow{Y_x V_x} = \overrightarrow{YV_x} = \begin{pmatrix} 1 \\ -6 \end{pmatrix}, \quad \overrightarrow{OX_x} = \begin{pmatrix} 1 \\ 0 \end{pmatrix}.$$

Furthermore,

$$\overrightarrow{X_x V_x} = M\overrightarrow{VY} = M\begin{pmatrix} -1 \\ 6 \end{pmatrix} = \begin{pmatrix} 56 \\ 25 \end{pmatrix}.$$

Finally, we solve (2-4-1) with $a = x$ to obtain

$$|Y_x V_x| = \tfrac{1}{19}(7+4\beta), \quad |X_x V_x| = \tfrac{1}{95}(3-\beta). \qquad \square$$

The next lemma allows us to compute the effect of k additional mutations at the corner Y.

Lemma 3.2.7. *While performing the sequence v^2yxy^k, for each of the final y mutations, the nodal ray $\vec{n}_Y$ always intersects the side $\overline{XV}$.*

Proof. We first compute the exact corners of the effect of the sequence v^2yx applied to Ω_β. From Lemma 3.2.6 we obtain the vertices $X = (1/\operatorname{vol}(\beta), 0) = \left(-1 + \frac{1}{3}\sqrt{30}, 0\right)$ and $Y = (0, \beta+3) = \left(0, \frac{1}{12}(42+5\sqrt{30})\right)$.

Let h_k denote the height of the quadrilateral along the y-axis after the mutation sequence v^2yxy^k, with $h_0 = \frac{1}{12}(42+5\sqrt{30})$ as above. Likewise, let (x_k, y_k) denote the vector $\vec{n}_Y$ at the vertex $(0, h_k)$ along which we are mutating, with $(x_0, y_0) = (1, -7)$ by Lemma 3.2.6, and let t_k denote the x-coordinate of the intersection point of the line through the point $(0, h_k)$ in the direction of the vector

(x_k, y_k) with the line through the point $\left(-1+\frac{1}{3}\sqrt{30}, 0\right)$ with slope $\frac{25}{56}$. In terms of h_k, x_k, and y_k, we can give t_k by the formula

$$t_k = \frac{x_k(168h_k + 25(\sqrt{30}-3))}{3(25x_k - 56y_k)}. \tag{3-2-2}$$

By definition of mutation, $h_k > h_{k-1}$ for all k. Assume by induction that $\vec{n}_Y$ intersects $\overrightarrow{XV}$ for the first $k-1$ mutations by y. Letting V_j denote the vertex V after the mutation sequence v^2yxy^{j-1}, our inductive hypothesis implies that V_j has both x and y coordinates less than V_{j-1} if $j < k$, so if $V_j = (x_v, y_v)$,

$$\frac{y_k}{x_k} < \frac{h_k - y_v}{x_v} < -6, \tag{3-2-3}$$

which is the slope of the initial side $\overrightarrow{YV}$.

Assume by way of contradiction that

$$t_k \leq -1 + \tfrac{1}{3}\sqrt{30}.$$

Using the formula in (3-2-2) for t_k, we have

$$\frac{x_k(168h_k + 25(\sqrt{30}-3))}{3(25x_k - 56y_k)} \leq \tfrac{1}{3}(-3+\sqrt{30}) \quad \Longleftrightarrow \quad h_k \leq \frac{(3-\sqrt{30})y_k}{3x_k}.$$

Then, by the inequality (3-2-3), we obtain

$$h_k \leq \frac{(3-\sqrt{30})y_k}{3x_k} < \tfrac{1}{3}(-6)(3-\sqrt{30}) = 2(\sqrt{30}-3).$$

However, $h_k \geq h_0 = \frac{1}{12}(42+5\sqrt{30})$ for all $k \in \mathbb{Z}_{\geq 0}$, and $h_0 = \frac{1}{12}(42+5\sqrt{30}) > 2(\sqrt{30}-3)$. Thus we have a contradiction. □

We now compute the nodal rays and directions of the sides after the mutation sequence v^2yxy^k.

Lemma 3.2.8. *After performing the sequence v^2yxy^k, the nodal rays are given by*

$$\vec{n}_Y = \begin{pmatrix} q_k \\ -p_k \end{pmatrix}, \quad \vec{n}_V = \begin{pmatrix} -q_{k-1} \\ p_{k-1} \end{pmatrix}, \quad \vec{n}_X = \begin{pmatrix} 11 \\ 5 \end{pmatrix},$$

and the direction vectors are given by

$$\overrightarrow{YV} = \begin{pmatrix} q_k^2 \\ -p_kq_k + 1 \end{pmatrix}, \quad \overrightarrow{XV} = \begin{pmatrix} 56 \\ 25 \end{pmatrix}.$$

Proof. We first must check the base case when $k = 0$, which was computed in Lemma 3.2.6. That is, by the defining recursion $x_k = 22x_{k-1} - x_{k-2}$, we have $p_{-1} = -1$ and $q_{-1} = 3$. For the inductive step, we explain how this lemma is equivalent to [Magill 2024, Lemma 6.6] and so follows by the proof there.

In [Magill 2024, Lemma 6.6], the lemma is similarly looking at y mutations to a quadrilateral where the nodal ray intersects the $|XV|\overrightarrow{XV}$ side of the polygon. The lemma assumes that the quadrilateral is defined via a triple $\mathcal{T}$ notated as $Q(\mathcal{T})$. Looking at the definition of $Q(\mathcal{T})$ in [Magill 2024, Definition 3.8], we see that if we set $\boldsymbol{E}_\lambda = \boldsymbol{E}_k$, $\boldsymbol{E}_\mu = \boldsymbol{E}_{k+1}$, and $\boldsymbol{E}_\rho = \boldsymbol{E}$, the definition for the nodal rays and direction vectors are the same as the identities we must prove. Further, after assuming which side the nodal ray will hit, checking formulas for nodal rays and direction vectors after a mutation do not depend on the side lengths. Thus, this lemma is equivalent to [Magill 2024, Lemma 6.6]. The proof uses the identities we already established in Lemma 3.2.3. □

Next we compute the affine lengths of the sides after the mutation sequence v^2yxy^k.

Lemma 3.2.9. *After performing the sequence v^2yxy^k, the affine lengths are given by*

$$|OY| = \frac{d_k + e_k\beta}{q_k}, \quad |OX| = -1 + \tfrac{1}{3}\sqrt{30} = \tfrac{1}{5}(4\beta - 7) = \frac{1}{\mathrm{vol}(\beta)},$$
$$|YV| = \frac{4\beta + 7}{q_k q_{k+1}}, \qquad |XV| = \frac{d_k - e_k\beta}{5q_{k+1}}.$$

Proof. We will show this by induction on k. The base case $k = 0$ is proved in Lemma 3.2.6. Suppose that the conclusions hold for k. Then, for $k+1$, by Lemma 3.2.7, in performing the consecutive y-mutations, the nodal ray will hit the $|XV|$ side of the polygon. Therefore, the $|OX|$ side remains constant.

For $|OY|$, it suffices to show that $|OY_y| = |OY| + |YV|$. By the induction hypothesis, we have

$$|OY| + |YV| = \frac{d_k + e_k\beta}{q_k} + \frac{4\beta + 7}{q_k q_{k+1}} = \frac{(q_{k+1}e_k + 4)\beta + (q_{k+1}d_k + 7)}{q_k q_{k+1}}.$$

It remains to show that $q_{k+1}e_k + 4 = q_k e_{k+1}$ and $q_{k+1}d_k + 7 = q_k d_{k+1}$. Both hold by induction. The base case is easily checked. For the inductive step, we show the details of the former, and the latter follows similarly. Assuming the equality holds for k, by Definition 3.0.1,

$$\begin{aligned} q_{k+1}e_k + 4 = (22q_k - q_{k-1})e_k + 4 &= 22q_k e_k - (q_{k-1}e_k - 4) \\ &= 22q_k e_k - q_k e_{k-1} = q_k(22e_k - e_{k-1}) = q_k e_{k+1}. \end{aligned}$$

This completes the proof for $|OY_y|$.

For $|XV_y|$, we must show

$$|XV_y| = \frac{d_{k+1} - e_{k+1}\beta}{5q_{k+2}}.$$

By adding the sides of the quadrilateral that is fixed during mutation, we have the equality

$$\begin{pmatrix} 0 \\ -|OY| \end{pmatrix} + \begin{pmatrix} |OX| \\ 0 \end{pmatrix} + |XV_y| \begin{pmatrix} 56 \\ 25 \end{pmatrix} = s \begin{pmatrix} q_k \\ -p_k \end{pmatrix},$$

where s is the length of the nodal ray $\vec{n}_Y$ where it intersects the side XV. This equality gives us two equations:

$$|OX| + 56|XV_y| = sq_k \quad \text{and} \quad -|OY| + 25|XV_y| = -sp_k.$$

We can solve the first one for s and substitute it into the second one to get the equation

$$-|OY| + 25|XV_y| = -\frac{p_k}{q_k}(|OX| + 56|XV_y|).$$

Solving for $|XV_y|$, we get

$$|XV_y| = \frac{q_k|OY| - p_k|OX|}{25q_k + 56p_k}.$$

First, we consider the denominator. We must show that

$$25q_k + 56p_k = q_{k+2}.$$

This follows from (3-1-6). We then consider the numerator where we substitute the formulas for $|OY|$ and $|OX|$:

$$q_k|OY| - p_k|OX| = (e_k\beta + d_k) - \tfrac{1}{5}p_k(4\beta - 7) = \tfrac{1}{5}(b(5e_k - 4p_k) + (5d_k + 7p_k)).$$

It remains to show that

$$-4p_k + 5e_k = -e_{k+1} \quad \text{and} \quad 5d_k + 7p_k = d_{k+1}.$$

Again, we prove the first identity by induction and the second follows similarly. The base case is easily checked. Suppose $4p_k - 5e_k = e_{k+1}$ for all k. Then, for $k+1$, by Definition 3.0.1,

$$\begin{aligned} 4p_{k+1} = 4(22p_k - p_{k-1}) &= 22(e_{k+1} + 5e_k) - (e_k + 5e_{k-1}) \\ &= (22e_{k+1} - e_k) + 5(22e_k - e_{k-1}) = e_{k+2} + 5e_{k+1}. \end{aligned}$$

It remains to show that the formula for $|YV|$ holds. We can verify this by checking the first equality in

$$\frac{4\beta + 7}{q_{k+1}q_{k+2}} = \frac{d_k - e_k\beta}{5q_{k+1}} - \frac{d_{k+1} - e_{k+1}\beta}{5q_{k+2}} = |VX| - |V_yX| = |Y_yV_y|.$$

This is equivalent to showing

$$\beta(-e_kq_{k+2} + e_{k+1}q_{k+1}) + (q_{k+2}d_k - d_{k+1}q_{k+1}) = 5(4\beta + 7).$$

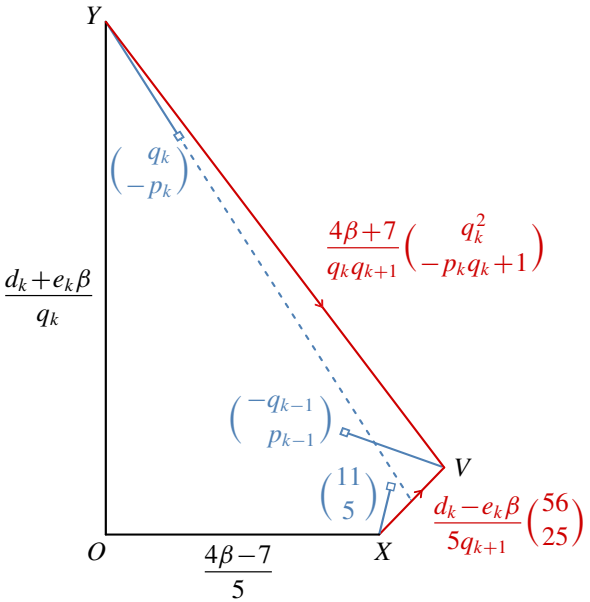

Figure 13. This figure illustrates Lemmas 3.2.8 and 3.2.9. The nodal rays are drawn in light blue, with a square indicating their marked point. The fact that $\vec{n}_Y$ intersects $\overrightarrow{XV}$ (Lemma 3.2.7) is indicated by the dashed blue line. The affine lengths of $|OX|$ and $|OY|$ are in black, while the vectors $|YV|\overrightarrow{YV}$ and $|XV|\overrightarrow{XV}$ are labeled in red, with their directions indicated by arrowheads.

Therefore, we must show that

$$-e_kq_{k+2}+e_{k+1}q_{k+1}=20 \quad \text{and} \quad q_{k+2}d_k-d_{k+1}q_{k+1}=35.$$

We prove the first identity here and the second follows in a similar manner. Suppose that, for all k, we have $-e_kq_{k+2}+e_{k+1}q_{k+1}=20$. Then, for $k+1$,

$$\begin{aligned}
-e_{k+1}q_{k+3}+e_{k+2}q_{k+2} &= -e_{k+1}(22q_{k+2}-q_{k+1})+e_{k+2}q_{k+2}\\
&= -22e_{k+1}q_{k+2}+e_{k+1}q_{k+1}+e_{k+2}q_{k+2}\\
&= -22e_{k+1}q_{k+2}+(20+e_kq_{k+2})+e_{k+2}q_{k+2}\\
&= 20-(22e_{k+1}-e_k)q_{k+2}+e_{k+2}q_{k+2}\\
&= 20-e_{k+2}q_{k+2}+e_{k+2}q_{k+2}=20.
\end{aligned}$$

□

See Figure 13 for an illustration of Lemmas 3.2.8 and 3.2.9. Together, these lemmas prove:

Proposition 3.2.10. *There is a full filling at the accumulation point. That is,*

$$c_\beta(\mathrm{acc}(\beta))=\mathrm{vol}(\beta).$$

Proof. By Lemmas 3.2.9 and 3.2.4, the sequence v^2yxy^k of mutations of the rectangle Ω_β is a convex quadrilateral containing the

$$\frac{d_k+e_k\beta}{q_k}\times\left(-1+\tfrac{1}{3}\sqrt{30}\right)=\frac{d_k+e_k\beta}{q_k}\times\frac{1}{\mathrm{vol}(\beta)}$$

right triangle abutting the axes. Multiplying by $\mathrm{vol}(\beta)$, we invoke Proposition 2.4.2 to obtain an embedding

$$(1-\varepsilon)\cdot E\left(1,\frac{\mathrm{vol}(\beta)(d_k+e_k\beta)}{q_k}\right)\overset{s}{\hookrightarrow}P(\mathrm{vol}(\beta),\mathrm{vol}(\beta)\beta)$$

for all $\varepsilon>0$. It therefore remains to show

$$\lim_{k\to\infty}\frac{\mathrm{vol}(\beta)(d_k+e_k\beta)}{q_k}=\mathrm{acc}(\beta).$$

First we note that

$$\mathrm{vol}(\beta)=\frac{5\mathrm{acc}(\beta)}{17+6\beta},\tag{3-2-4}$$

which can be checked using the formulas for β and $\mathrm{acc}(\beta)$ in (3-0-1). Thus our goal becomes

$$\lim_{k\to\infty}\frac{d_k+e_k\beta}{q_k}=\tfrac{1}{5}(17+6\beta).$$

We find a closed form for the recursion $x_k=22x_{k-1}-x_{k-2}$ with $x_k=d_k,e_k,q_k$. Set

$$r=11+2\sqrt{30},\quad d=\tfrac{3}{2}+\tfrac{31}{120}\sqrt{30},\quad e=\tfrac{1}{2}+\tfrac{1}{10}\sqrt{30},\quad q=\tfrac{1}{2}+\tfrac{1}{15}\sqrt{30},$$
$$\bar{d}=\tfrac{3}{2}-\tfrac{31}{120}\sqrt{30},\quad \bar{e}=\tfrac{1}{2}-\tfrac{1}{10}\sqrt{30},\quad \bar{q}=\tfrac{1}{2}-\tfrac{1}{15}\sqrt{30}.$$

Then

$$d_k=dr^k+\bar{d}r^{-k},\quad e_k=er^k+\bar{e}r^{-k},\quad q_k=qr^k+\bar{q}r^{-k}.$$

Then we have

$$\begin{aligned}\lim_{k\to\infty}\frac{d_k+e_k\beta}{q_k}&=\lim_{k\to\infty}\frac{dr^k+\bar{d}r^{-k}+(er^k+\bar{e}r^{-k})b}{qr^k+\bar{q}r^{-k}}\\&=\lim_{k\to\infty}\frac{d+\bar{d}r^{-2k}+(e+\bar{e}r^{-2k})b}{q+\bar{q}r^{-2k}}=\frac{d+e\beta}{q}=\tfrac{1}{5}(17+6\beta).\end{aligned}$$

□

Remark 3.2.11. Notice that the slope of $\overrightarrow{YV}$ has limit

$$\lim_{k\to\infty}\frac{p_kq_k-1}{q_k^2}=\lim_{k\to\infty}\frac{p_k}{q_k}=\mathrm{acc}(\beta)$$

by Corollary 3.1.6. Coupled with the fact that

$$\overrightarrow{XV}=\frac{d_k-e_k\beta_k}{5q_{k+1}}\begin{pmatrix}56\\25\end{pmatrix},$$

to prove Proposition 3.2.10, it would suffice to show that $d_k/e_k \to \beta$, so that the short side $\overrightarrow{XV}$ approaches zero and thus the ratio $|OY|/|OX|$ approaches the slope of $\overrightarrow{YV}$. However, this would also require solving the recursion.

To get the points on the capacity function, we now consider the sequence $v^2yxy^kxy^2$. This allows us to prove Proposition 3.0.6 and support Conjecture 3.0.7, because

- the sequence of mutations v^2yxy^kxy provides an embedding realizing the inner corner between the obstructions from $\boldsymbol{E}_k$ and $\hat{\boldsymbol{E}}_{k+1}$, while
- the sequence of mutations $v^2yxy^kxy^2$ conjecturally provides an embedding realizing the inner corner between the obstructions from $\hat{\boldsymbol{E}}_{k+1}$ and $\boldsymbol{E}_{k+1}$.

We will use the notation

$$d' := 2q - d, \quad e' := 2q - e.$$

In the following lemma, we are going to use no subscripts to denote the vertices from v^2yxy^k, and then add a subscript of x to get the vertices from v^2yxy^kx.

Lemma 3.2.12. *Beginning with the data from Lemma 3.2.9 from performing the sequence v^2yxy^k, one mutation by x gives the nodal rays*

$$\vec{n}_{Y_x} = \begin{pmatrix} q_k \\ -p_k \end{pmatrix}, \quad \vec{n}_{V_x} = \begin{pmatrix} -11 \\ -5 \end{pmatrix}, \quad \vec{n}_{X_x} = \begin{pmatrix} 121p_{k-1} + 54q_{k-1} \\ 56p_{k-1} + 25q_{k-1} \end{pmatrix},$$

the direction vectors

$$\overrightarrow{Y_xV_x} = \begin{pmatrix} q_k^2 \\ -p_kq_k + 1 \end{pmatrix}, \quad \overrightarrow{X_xV_x} = \begin{pmatrix} -54q_k^2 - 121p_kq_k + 121 \\ -25q_k^2 - 56p_kq_k + 56 \end{pmatrix},$$

and the affine lengths

$$|OY_x| = \frac{d_k + e_k\beta}{q_k}, \qquad |OX_x| = \frac{d'_{k+1} + e'_{k+1}\beta}{q_{k+1}},$$
$$|Y_xV_x| = \frac{-d'_{k+1} + e'_{k+1}\beta}{q_k\hat{q}_{k+1}}, \quad |X_xV_x| = \frac{d_k - e_k\beta}{q_{k+1}\hat{q}_{k+1}}.$$

Proof. We first give the proof for the direction vectors and nodal rays.

By Lemma 3.2.8, after performing the sequence v^2yxy^k, we have $\vec{n}_X = (11, 5)$, $\vec{n}_V = (-q_{k-1}, p_{k-1})$, and $\overrightarrow{XV} = (56, 25)$. Note that, for the next mutation at X, because $\vec{n}_X$ has positive slope, it will always hit the edge $\overrightarrow{YV}$. Thus, the mutation matrix should satisfy

$$M\vec{n}_X = \vec{n}_X, \quad M\overrightarrow{XV} = \overrightarrow{OX} \iff M = \begin{pmatrix} -54 & 121 \\ -25 & 56 \end{pmatrix}.$$

The polygon after mutation at X should thus have $\vec{n}_{Y_x} = \vec{n}_Y$,

$$\vec{n}_{V_x} = -\vec{n}_X = \begin{pmatrix} -11 \\ -5 \end{pmatrix}, \quad \vec{n}_{X_x} = M\vec{n}_V = \begin{pmatrix} 121p_{k-1} + 54q_{k-1} \\ 56p_{k-1} + 25q_{k-1} \end{pmatrix},$$

and

$$\overrightarrow{X_xV_x} = -M\overrightarrow{YV} = \begin{pmatrix} -54q_k^2 - 121p_kq_k + 121 \\ -25q_k^2 - 56p_kq_k + 56 \end{pmatrix},$$

while $\overrightarrow{Y_xV_x} = \overrightarrow{YV}$ because $\vec{n}_X$ hits $\overrightarrow{YV}$.

We now give the proofs for the affine lengths. Note that $|OY_x| = |OY|$ because $Y_x = Y$. Next, to compute $|OX_x|$, we check that, given the formulas for $|OX|$ and $|XV|$ from Lemma 3.2.9, we have

$$|OX_x| = |OX| + |XV| = \tfrac{1}{5}(4\beta - 7) + \frac{d_k - e_k\beta}{5q_{k+1}} = \frac{d'_{k+1} + e'_{k+1}\beta}{q_{k+1}}.$$

This follows from the identities

$$4q_{k+1} - e_k = 5e'_{k+1} \quad \text{and} \quad -7q_{k+1} + d_k = 5d'_{k+1},$$

which hold by induction because they are linear identities and the (d_k, e_k, q_k) (and thus d'_k and e'_k) satisfy the same linear recursion.

We now look at $|Y_xV_x|$. Following the proof of [Magill 2024, Lemma 6.1 (ii)] (which solves for $|Y_xV_x|$ using the fact that the sides of the quadrilateral which is fixed under x-mutation, with sides $|OX|\overrightarrow{OX}$, $-|Y_xV_x|\overrightarrow{YV}$, $|OY_x|\overrightarrow{OY}$, and a side parallel to $\vec{n}_X$, must add to zero), the stated formula for $|Y_xV_x|$ holds if our analogue of [Magill 2024, (6.0.2)] gives us the claimed value for $|Y_xV_x|$, that is,

$$|Y_xV_x| = \frac{11|OY| + 5|OX|}{-11 + q_k(41p_k + 5q_k - 30p_k)} = \frac{-d'_{k+1} + e'_{k+1}\beta}{q_k\hat{q}_{k+1}}. \tag{3-2-5}$$

For the denominator of (3-2-5), note that

$$-11 + q_k(41p_k + 5q_k - 30p_k) \overset{(*)}{=} t_{k+1}q_k - 11 \overset{(**)}{=} t_kq_{k+1} - 5 = \hat{q}_{k+1},$$

where $(*)$ uses Lemma 3.2.3 (iv), and where $(**)$ uses the second conclusion of Lemma 3.2.3 (ii), both applied to $(\boldsymbol{E}_k, \boldsymbol{E}_{k+1}, \boldsymbol{E})$.

For the numerator of (3-2-5), we must show

$$11|OY| + 5|OX| = (-d'_{k+1} + e'_{k+1}\beta)/q_k.$$

We have

$$11|OY| + 5|OX| = \frac{11(d_k + e_k\beta)}{q_k} + (4\beta - 7),$$

so we must check that

$$11e_k + 4q_k = e'_{k+1} \quad \text{and} \quad 11d_k - 7q_k = -d'_{k+1}.$$

As in the proof of the $|OX_x|$ formula, these hold by induction, using the fact that all terms satisfy the same recursion.

Finally, to verify the formula for $|X_xV_x|$, we check that

$$|X_xV_v| = |YV| - |Y_xV_x| = \frac{4\beta+7}{q_kq_{k+1}} - \frac{-d'_{k+1}+e'_{k+1}\beta}{q_k\hat{q}_{k+1}} = \frac{d_k-e_k\beta}{q_{k+1}\hat{q}_{k+1}}.$$

This is equivalent to

$$4\hat{q}_{k+1} - e'_{k+1}q_{k+1} = -e_kq_k \quad \text{and} \quad 7\hat{q}_{k+1} + d'_{k+1}q_{k+1} = d_kq_k.$$

The first formula can be verified as follows:

$$\begin{aligned}
4\hat{q}_{k+1} - e'_{k+1}q_{k+1} &= -e_kq_k, \\
4(22t_kq_{k+1}-5) - (2q_{k+1}-e_{k+1})q_{k+1} &= -e_kq_k, \\
16t_kq_{k+1} - 80 - 7q_{k+1} + p_{k+1}q_{k+1} - t_{k+1}q_{k+1} &= -p_kq_k - q_k^2 + t_kq_k \quad \text{(Lem. 2.2.5)}, \\
-6t_kq_{k+1} + 30 - 7q_{k+1} + p_{k+1}q_{k+1} &= -p_kq_k - q_k^2 \quad \text{(Lem. 3.2.3 (v))}, \\
5t_kq_{k+1} + 30 - 22q_kq_{k+1} &= -p_kq_k - q_k^2 \quad \text{(Lem. 3.2.3 (iii))}, \\
t_kq_{k+1} + 6 &= t_{k+1}q_k \quad \text{(Lem. 3.2.3 (i))},
\end{aligned}$$

which holds by Lemma 3.2.3 (ii). All applications of Lemma 3.2.3 use the triple $(\boldsymbol{E}_k, \boldsymbol{E}_{k+1}, \boldsymbol{E})$. The verification of the second formula uses the exact same sequence of identities. □

The next lemma is the key step which allows us to prove Proposition 3.0.6 and thus Theorem 1.1.1. Similar to Lemma 3.2.12, we use no subscripts to denote the vertices after the sequence v^2yxy^kx, and a subscript y to denote the vertices after the final y mutation.

Lemma 3.2.13. *After performing the sequence of mutations v^2yxy^kxy, the affine lengths of the axis sides are*

$$|OY_y| = \frac{\hat{d}_{k+1}+\hat{e}_{k+1}\beta}{\hat{q}_{k+1}} \quad \textit{and} \quad |OX_y| = \frac{d_k+e_k\beta}{p_k}.$$

Proof. First we show that, for the last y-mutation, $\vec{n}_Y$ extends to hit the side $\overrightarrow{OX}$ (rather than $\overrightarrow{XV}$ as for earlier y-mutations in Lemmas 3.2.6 and 3.2.7). As a consequence, we prove the formula for $|OX_y|$. By Lemma 3.2.12, we need to show that

(i) the x-coordinate of the x-intercept of the line of slope $-p_k/q_k$ (the slope of $\vec{n}_Y$) through the point $(0, |OY|) = (0, (d_k+e_k\beta)/q_k)$ is less than $|OX| = (d'_{k+1}+e'_{k+1}\beta)/q_{k+1}$, and that

(ii) this x-coordinate equals the claimed value $(d_k+e_k\beta)/p_k$ of $|OX_y|$.

Note that this x-coordinate is at the solution to

$$-\frac{d_k+e_k\beta}{q_k}=-\frac{p_k}{q_k}x \quad\Longleftrightarrow\quad x=\frac{d_k+e_k\beta}{p_k},$$

so proving (i) suffices to prove (ii). To prove (ii), we need to show

$$\frac{d_k+e_k\beta}{p_k}<\frac{d'_{k+1}+e'_{k+1}\beta}{q_{k+1}}. \tag{3-2-6}$$

Recall that in Proposition 3.2.10, we solved the recursion defining the $\boldsymbol{E}_k$ and found

$$\begin{aligned} r&=11+2\sqrt{30}, \quad & d&=\tfrac{3}{2}+\tfrac{31}{120}\sqrt{30}, \quad & e&=\tfrac{1}{2}+\tfrac{1}{10}\sqrt{30}, \quad & q&=\tfrac{1}{2}+\tfrac{1}{15}\sqrt{30},\\ & & \bar{d}&=\tfrac{3}{2}-\tfrac{31}{120}\sqrt{30}, \quad & \bar{e}&=\tfrac{1}{2}-\tfrac{1}{10}\sqrt{30}, \quad & \bar{q}&=\tfrac{1}{2}-\tfrac{1}{15}\sqrt{30}. \end{aligned}$$

We can further compute

$$p=\tfrac{7}{2}+\tfrac{13}{20}\sqrt{30}, \quad \bar{p}=\tfrac{7}{2}-\tfrac{13}{20}\sqrt{30}.$$

Expanding (3-2-6) using $x_k=xr^k+\bar{x}r^{-k}$ for $x=d,e,p,q$, we want to show

$$c_{2k+1}r^{2k+1}+c_1r+c_{-1}r^{-1}+c_{-2k-1}r^{-2k-1}>0,$$

where

$$\begin{aligned} c_{2k+1}&=(2q-d)p+(2q-e)p\beta-dq-eq\beta=0,\\ c_1&=(2q-d)\bar{p}+(2q-e)\bar{p}\beta-\bar{d}q-\bar{e}q\beta=-\tfrac{17}{12}+\tfrac{31}{120}\sqrt{30}\approx-0.0017,\\ c_{-1}&=(2\bar{q}-\bar{d})p+(2\bar{q}-\bar{e})p\beta-d\bar{q}-e\bar{q}\beta=\tfrac{27}{8}+\tfrac{37}{60}\sqrt{30}\approx 6.7526, \text{ and}\\ c_{-2k-1}&=(2\bar{q}-\bar{d})\bar{p}+(2\bar{q}-\bar{e})\bar{p}\beta-\bar{d}\bar{q}-\bar{e}\bar{q}\beta=-\tfrac{215}{24}+\tfrac{39}{24}\sqrt{30}\approx-0.0578. \end{aligned}$$

Because $c_{2k+1}=0,\ r>1,\ k\geq 0$, and $c_{-2k-1}<0$, for all $k\geq 1$,

$$c_{2k+1}r^{2k+1}+c_1r+c_{-1}r^{-1}+c_{-2k-1}r^{-2k-1}>c_1r+c_{-1}r^{-1}+c_{-2k-1}r^{-2(k-1)-1},$$

which means

$$\begin{aligned} c_{2k+1}r^{2k+1}+c_1r+c_{-1}r^{-1}+c_{-2k-1}r^{-2k-1}&>c_1r+(c_{-1}+c_{-2k-1})r^{-1}\\ &=-196+215\sqrt{\tfrac{5}{6}}\approx 0.2673>0. \end{aligned}$$

Finally we prove the statement about $|OY_y|$. By Lemma 3.2.12, we must verify that

$$|OY_y|=|OY|+|YV|=\frac{d_k+e_k\beta}{q_k}+\frac{-d'_{k+1}+e'_{k+1}\beta}{q_k\hat{q}_{k+1}}=\frac{\hat{d}_{k+1}+\hat{e}_{k+1}\beta}{\hat{q}_{k+1}}.$$

Therefore, the formula for $|OY|$ will hold if

$$e'_{k+1}=q_k\hat{e}_{k+1}-\hat{q}_{k+1}e_k \quad\text{and}\quad d'_{k+1}=\hat{q}_{k+1}d_k-q_k\hat{d}_{k+1}.$$

Using Remark 3.2.5 and Lemma 2.2.5 to replace all d, e terms with p, q, t, the first identity becomes

$$\begin{aligned} 7q_{k+1} - p_{k+1} + t_{k+1} &= q_k\hat{p}_{k+1} + q_k\hat{q}_{k+1} - q_k\hat{t}_{k+1} - \hat{q}_{k+1}p_k - \hat{q}_{k+1}q_k + \hat{q}_{k+1}t_k, \\ 7q_{k+1} - p_{k+1} &= -q_k\hat{t}_{k+1} + \hat{q}_{k+1}t_k \qquad \text{(Lem. 3.2.3 (vii))}, \end{aligned}$$

which holds by Lemma 3.2.3 (ii). (Both uses of Lemma 3.2.3 (vii) are applied to the triple $(\boldsymbol{E}_k, \hat{\boldsymbol{E}}_{k+1}, \boldsymbol{E}_{k+1})$.) The proof of the second identity is almost identical. □

Remark 3.2.14. Note that in Lemma 3.2.13 the nodal ray of the additional y mutation hits the side OX of the quadrilateral rather than the side XV like in Lemma 3.2.9. This implies the formulas in Lemma 3.2.13 are no longer in parallel with the formulas derived in [Magill 2024]. Instead, as found in [Magill ≥ 2025], when the nodal ray emanating from Y changes the side it intersects with, this corresponds to moving from an embedding strictly above the function to one that lies on the function.

We prove Proposition 3.0.6, proving that there is a full filling at the inner corner between the obstructions from $\boldsymbol{E}_k$ and $\hat{\boldsymbol{E}}_{k+1}$.

Proof of Proposition 3.0.6. By Lemma 3.2.13, there is an embedding

$$(1-\varepsilon)\cdot E\left(\frac{d_k + e_k\beta}{p_k}, \frac{\hat{d}_{k+1} + \hat{e}_{k+1}\beta}{\hat{q}_{k+1}}\right) \overset{s}{\hookrightarrow} P(1,\beta)$$

for all $\varepsilon > 0$. Thus there is an embedding

$$E\left(1, \frac{p_k(\hat{d}_{k+1} + \hat{e}_{k+1}\beta)}{\hat{q}_{k+1}(d_k + e_k\beta)}\right) \overset{s}{\hookrightarrow} \frac{1}{1-\varepsilon}\cdot P\left(\frac{p_k}{d_k + e_k\beta}, \frac{p_k\beta}{d_k + e_k\beta}\right),$$

implying that

$$c_\beta\left(\frac{p_k(\hat{d}_{k+1} + \hat{e}_{k+1}\beta)}{\hat{q}_{k+1}(d_k + e_k\beta)}\right) \leq \frac{p_k}{d_k + e_k\beta}$$

once we take the infimum defining c_β. □

To close this section, we explain our reasoning behind Conjecture 3.0.7.

Remark 3.2.15. We initially believed that

$$c_\beta|_{[1,\mathrm{acc}(\beta)]} = \sup_k\{\mu_{\boldsymbol{E}_k,\beta}|_{[1,\mathrm{acc}(\beta)]}\}$$

and thought that Theorem 1.1.1 would be proved as a consequence of the lower bounds from Proposition 3.0.4 (i) and an embedding providing an upper bound at the intersection between the horizontal line through O_{k-1} and the line through the origin and O_k (see Figure 11 or 15). Specifically, we thought there might be an infinite sequence of mutations starting with v^2yxy^kxy which approached this hypothetical inner corner. We held on to this expectation because the obstructions from the

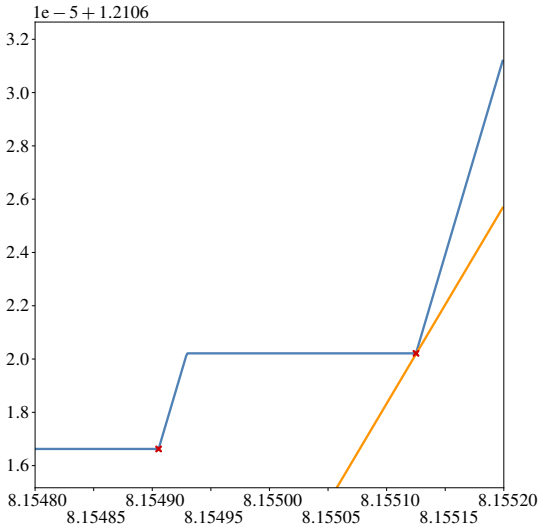

Figure 14. Here we have depicted the obstruction from the inner class $\hat{\boldsymbol{E}}_1$. The orange curve is the volume obstruction $\mathrm{vol}_\beta(z)$, and the embedding function c_β is in blue. The red $\times$ on the left depicts the embedding from the mutation sequence v^2yx^2y proving Proposition 3.0.6, while the $\times$ on the right depicts the embedding from the mutation sequence $v^2yx^2y^2$ supporting Conjecture 3.0.7.

classes $\hat{\boldsymbol{E}}_k$ are extremely difficult to visualize computationally.[8] The obstruction from $\hat{\boldsymbol{E}}_2$ corresponds to the 4, 769, 607, 569-th ECH capacity by Lemma 2.3.5, while comparing the ratios between even the first 10, 000, 000 ECH capacities is very computationally expensive! See Figure 14 for the (simplest) $\hat{\boldsymbol{E}}_1$.

By comparison with [Usher 2019] and through personal communication with Usher, we eventually discovered the inner classes $\hat{\boldsymbol{E}}_k$ and found the same sequence considered in [Magill $\geq$ 2025], namely v^2yxy^kxy, proves Proposition 3.0.6. In order to compute all of c_β on $[1, \mathrm{acc}(\beta)]$, we would need to prove Conjecture 3.0.7 by identifying a sequence of mutations of $P(1, \beta)$ such that

$$|OX| = \frac{\hat{d}_{k+1} + \hat{e}_{k+1}\beta}{\hat{p}_{k+1}}, \quad |OY| = \frac{d_{k+1} + e_{k+1}\beta}{q_{k+1}}.$$

Our hypothesized sequence of mutations is $v^2yxy^kxy^2$, which would provide a full filling and thus upper bound for c_β at the inner corner between the obstructions from $\hat{\boldsymbol{E}}_{k+1}$ and $\boldsymbol{E}_{k+1}$: in Figure 15, this would mean that c_β equals the dashed black line.

[8] We also naively failed to notice that the intersection between the obstructions from $\boldsymbol{E}_0$ and $\boldsymbol{E}_1$ is below the volume obstruction. This is not true for all k, however.

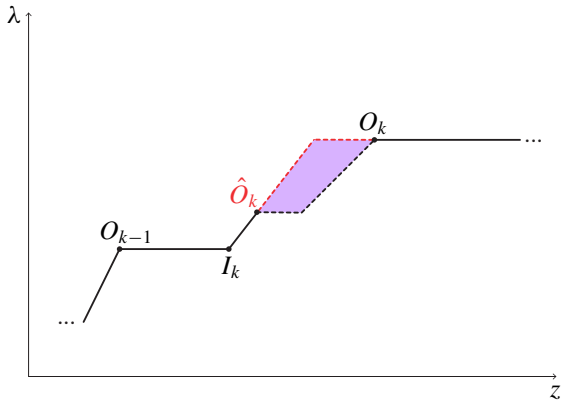

Figure 15. This figure provides more detail on the schematic presented in Figure 10. Using Propositions 3.0.4 (i), (ii), and 3.0.6, along with Lemma 3.0.8 (i), we have computed c_β along the solid black lines. However, we would need to prove Conjecture 3.0.7 to compute c_β in between $\hat{O}_k$ and O_k. We know the function must lie in the violet quadrilateral (possibly on its boundary), and we conjecture the function is given by its lower boundary, the dashed black line.

However, computing $|OX|$ and $|OY|$ for the sequence $v^2yxy^kxy^2$ — even though it differs from the sequence v^2yxy^kxy considered in Lemma 3.2.13 by only one y-mutation — is considerably more time consuming because for the final two y mutations, the nodal ray $\vec{n}_Y$ hits the bottom side OX of the quadrilateral rather than the side XV that the previous y^k mutations hit. Thus, to determine the combinatorics for the quadrilaterals of the y mutations hitting the side OX would involve many new computations. While this could be done, computing the whole function is not necessary to claim there is an infinite staircase.

4. Other properties of the embedding function

In this section we collect several observations about the structure of the ellipsoid embedding function for polydisks which may be useful for future work.

4.1. ***Towards Conjecture 1.1.2.*** Proving Conjecture 1.1.2 would require analogues of Propositions 3.0.4 (i) and 3.0.6. For the obstructions providing the outer corners, this means identifying new Diophantine classes and proving that they are Diophantine. In analogy to [Magill et al. 2024], we expect that the correct classes $\boldsymbol{E}_{k,n}$ and $\hat{\boldsymbol{E}}_{k,n}$ can be obtained from $\boldsymbol{E}_{k,2} := \boldsymbol{E}_k$ and $\hat{\boldsymbol{E}}_{k,2} := \hat{\boldsymbol{E}}_k$ as follows:

- Modify $p_{k,2}/q_{k,2} := p_k/q_k$ by adding $2n-4$ to each entry in its continued fraction; this is $p_{k,n}/q_{k,n}$.
- Use Lemma 2.2.5 to define $d_{k,n}$ and $e_{k,n}$.

To prove the analogue of Proposition 3.0.6 requires identifying new embeddings. In analogy to [Magill 2024] we expect that this amounts to performing the mutations v^n at the start of every sequence of mutations from in Section 3.2, rather than just v^2.

It would also be possible to prove Conjecture 1.1.2 using [Usher 2019, Theorem 4.4]. However, this would require proving that the Diophantine quasiperfect classes $\boldsymbol{E}_{k,n}$ are perfect,[9] which we do not do in this paper.

Finally we discuss the obstructions analogous to $\boldsymbol{E}$ appearing after the accumulation point of the conjectural staircases c_{β_n}.

Remark 4.1.1. (i) We predict that the ECH capacity which gives the step after the accumulation point, generalizing the obstruction for $\boldsymbol{E}$ in the case $n = 2$, for the infinite staircases of Conjecture 1.1.2 will have index

$$k_n = (2n+1)(2n^2+6n+5) = 4n^3+14n^2+16n+5$$

for $n \geq 2$. At these steps, the z-coordinate of the associated outer corner is given by the fraction p_n/q_n, where

$$p_n = 4n^2+10n+5 \quad \text{and} \quad q_n = 2n+1.$$

The first few of these values are summarized in the following table:

n	p_n	q_n	k_n
2	41	5	125
3	71	7	287
4	109	9	549
5	155	11	935
6	209	13	1469

One can check, using the formulas for p_n, q_n, and k_n above, that

$$k_n = \tfrac{1}{2}(p_n+1)(q_n+1) - 1$$

for every $n \geq 2$, as predicted by the proof of Lemma 2.3.5.

Also, note that

$$p_n + q_n = 2(2n^2+6n+3) = t_{n+1},$$

which is the predicted coefficient of the recursion governing the outer corners of the next infinite staircase in this family.

(ii) Another way to identify the steps after the accumulation point is to compare to the case of H_b and use Conjecture 1.2.1. For H_b, these steps are the obstructions

[9] For a class to be *perfect*, it must be represented by a symplectically embedded sphere, rather than one that is only immersed. That the classes $\boldsymbol{E}_{k,n}$ and $\hat{\boldsymbol{E}}_{k,n}$ are quasiperfect can be proved following the $n = 2$ case discussed in the proof of Proposition 3.0.4.

from the quasiperfect Diophantine classes centered at[10]

$$[7,4],\ [9,6],\ \ldots,\ [2n+3,2n].$$

Thus, for $P(1,\beta)$, we expect the centers to be at $[2n+4,2n+1]$. This agrees with the p_n and q_n computed in (i):

$$[2n+4,2n+1]=2n+4+\frac{1}{2n+1}=\frac{(2n+4)(2n+1)+1}{2n+1}.$$

We can then use

$$t_n=\sqrt{p_n^2-6p_nq_n+q_n^2+8}$$

and Lemma 2.2.5 to identify the corresponding quasiperfect Diophantine classes

$$\boldsymbol{E}_n:=(2n^2+4n+1,\ 2n+2,\ 4n^2+10n+5,\ 2n+1,\ 2(2n^2+2n-1)).$$

Notice $\boldsymbol{E}_2$ is what we have been referring to as $\boldsymbol{E}$.

(iii) The relevance of the $\boldsymbol{E}_n$ to the staircases c_{β_n} can also be seen in the fact that the obstruction $\mu_{\boldsymbol{E}_n,\beta_n}(z)$ crosses through the volume obstruction $\mathrm{vol}_{\beta_n}(z)$ at $z=\mathrm{acc}(\beta_n)$. That is,

$$\mu_{\boldsymbol{E}_n,\beta_n}(\mathrm{acc}(\beta_n))=\frac{q_n\mathrm{acc}(\beta_n)}{d_n+e_n\beta_n}=\sqrt{\frac{\mathrm{acc}(\beta_n)}{2\beta_n}}=\frac{1+\mathrm{acc}(\beta_n)}{2+2\beta_n}=\mathrm{vol}(\beta_n),$$

implying that (3-2-1) holds with q_n, d_n, and e_n replacing q, d, and e. We won't prove either of these claims here, but we do note that it is a straightforward if tedious computation using the formulas for β_n and $\mathrm{acc}(\beta_n)$ in Conjecture 1.1.2 and for q_n, d_n, and e_n in (ii) above.

4.2. ***Usher's conjecture.*** Usher [2019] considers the family

$$L_{n,0}:=\sqrt{n^2-1},$$

proving that $c_{L_{n,0}}$ has an infinite staircase. He does this by proving that a sequence of classes $A_{k,n}$ are perfect.[11]

Usher's classes $A_{k,n}$ play the role of our classes $\boldsymbol{E}_k$ (or $\boldsymbol{E}_{k,n}$ more generally). However, he also identified other obstructions

$$\hat{A}_{k,n}:=t_{k-1,n}A_{k,n}-\boldsymbol{E}(n),$$

where $\boldsymbol{E}(n):=\boldsymbol{E}=(n+1,1,2n+3,1,2n)$.[12]

[10]Here we are starting with $n=2$ as in [Usher 2019], as opposed to $n=0$ as in [Bertozzi et al. 2021; Magill et al. 2024].

[11]Again note that we use k to denote a step of the staircase where Usher uses i.

[12]Note that the $\hat{A}_{k,n}$ are not defined in precisely this way in [Usher 2019, §4.6]; this definition is inspired by "x-mutation" investigated in [Magill et al. 2024]. His k-indexing of the $\hat{A}_{k,n}$ classes is also one less than what we define here.

The classes $\boldsymbol{E}(n)$ are similar to our $\boldsymbol{E} = (17, 6, 41, 5, 22)$. Our new staircase c_β accumulates to precisely the point where the obstruction from $\boldsymbol{E}$ for $z < \frac{41}{5}$ crosses the volume curve; see (3-2-4). Meanwhile, Usher's staircases satisfy

$$\mu_{\boldsymbol{E}(n),L_{n,0}}(\mathrm{acc}(L_{n,0})) = \frac{\mathrm{acc}(L_{n,0})}{n+1+L_{n,0}} = \mathrm{vol}_{L_{n,0}}(\mathrm{acc}(L_{n,0})).$$

Usher conjectured he could compute the whole function up to the accumulation point. He conjectures the following.

Conjecture 4.2.1 [Usher 2019, Conjecture 4.23]. *Between the center of $A_{0,n}$ and* $\mathrm{acc}(L_{n,0})$, $c_{L_{n,0}}$ *equals the supremum of the obstructions $\mu_{\boldsymbol{E},L_{n,0}}$, where $\boldsymbol{E}$ is one of the $A_{k,n}$ or $\hat{A}_{k,n}$.*

Our proof of Theorem 1.1.1 (i) proves that c_β is determined on $[p_k/q_k, \hat{p}_{k+1}/\hat{q}_{k+1}]$ by only the classes $\boldsymbol{E}_k$ and $\hat{\boldsymbol{E}}_k$; proving Conjecture 3.0.7 would solve our version of Usher's conjecture. We expect that Usher's conjecture for the $c_{L_{n,0}}$ staircases could be solved by proving:

- the analogue of Proposition 3.0.6 using the mutation sequence $v^{n-1}y^{k+1}xy$ to compute the inner corner between $A_{k,n}$ and $\hat{A}_{k+1,n}$,
- the analogue of Conjecture 3.0.7 using the mutation sequence $v^{n-1}y^{k+1}xy^2$ to compute the inner corner between $\hat{A}_{k+1,n}$ and $A_{k+1,n}$.

4.3. ***Descending staircases and fractal structure.*** If Conjecture 1.2.1 is true, then the set of $\sqrt{3} < \beta \leq \sqrt{8}$ for which c_β has an infinite staircase is homeomorphic to the Cantor set. Key to proving this analogy is understanding how c_β with $\beta = \frac{1}{12}(6+5\sqrt{30})$ can be obtained from $c_{\sqrt{8}}$ and a descending infinite staircase c_β "mirroring" $c_{\sqrt{3}}$.

In fact, the descending staircase with

$$\beta = \tfrac{1}{13}(24+7\sqrt{3})$$

was one of the first conjectural infinite staircases we found via computer exploration, and it is precisely this mirror! It is shown in Figure 16. The reason why we think of $\beta = \frac{1}{13}(24+7\sqrt{3})$ and $\sqrt{3}$ as paired is that both accumulate to the point where the obstruction from $(3, 1, 7, 1, 4)$ intersects the volume curve $\mathrm{vol}_\beta(z)$; the ascending staircase $c_{\sqrt{3}}$ from below, where the obstruction has positive slope, and the descending staircase c_β from above, where the obstruction is horizontal.

The first two steps of c_β are $(5, 1, 9, 1, 6)$ and $\boldsymbol{E} = (17, 6, 41, 5, 22)$. These three classes form what is called in [Magill et al. 2024] a "compatible triple". Thus we expect the same Cantor set structure to arise for $P(1, \beta)$ infinite staircases with $7 < \mathrm{acc}(\beta) < 9$ as it does for the target H_b with $6 < \mathrm{acc}_H(b) < 8$, see [Magill et al. 2024, Theorem 1.1.1].

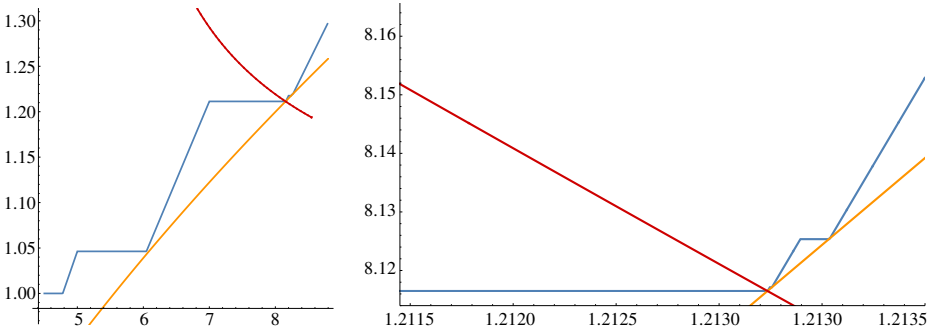

Figure 16. Here we depict the conjectural infinite staircase c_β with $\beta = \frac{1}{13}(24+7\sqrt{3})$. In both figures, $\mathrm{vol}_\beta(z)$ is orange and c_β is blue. The accumulation point curve $(\mathrm{acc}(\beta), \mathrm{vol}(\beta))$ is in red with β varying. Thus the accumulation point of c_β ought to occur at the intersection of these three curves. The figure on the left suggests that the accumulation point is precisely where the horizontal obstruction from the class $(3, 1, 7, 1, 4)$ intersects the volume curve. On the right, we have zoomed in.

Moreover, the language of "blocking classes" developed in [Bertozzi et al. 2021] and relying on the accumulation point formula from [Cristofaro-Gardiner et al. 2020] provides more detail for understanding the results of [Cristofaro-Gardiner et al. 2017]. In Section 2.1 we defined the notion of a blocked β-value. Using the lower bound (2-2-2) on c_β by the obstructions $\mu_{\boldsymbol{E},\beta}$, we say a quasiperfect Diophantine class $\boldsymbol{E}$ *blocks* c_β from having an infinite staircase if $\mu_{\boldsymbol{E},\beta}(\mathrm{acc}(\beta)) > \mathrm{vol}_\beta(\mathrm{acc}(\beta))$. We expect that c_n, $n \in \mathbb{Z}_{\geq 2}$ are blocked by the perfect classes $\boldsymbol{E}(n)$. This illustrates the power of [Cristofaro-Gardiner et al. 2020, Theorem 1.13]: it reaffirms why the classes $\boldsymbol{E}(n)$ — which appeared in different notation as the classes E_n in [Cristofaro-Gardiner et al. 2017, (1-4)] — are natural key players for the computations of Cristofaro-Gardiner, Frenkel, and Schlenk.

4.4. ***Brahmagupta moves.*** In [Magill and McDuff 2023; Magill et al. 2024; Usher 2019], the authors found a symmetry, referred to as a Brahmagupta move by [Usher 2019], that acts on quasiperfect classes to construct infinitely many different targets that have infinite staircases given one target with an infinite staircase.

It is more natural to define these symmetries via their action on the z-variable than the β-variable in the case of the polydisk (or the b-variable in the case of the Hirzebruch surface). Given an infinite sequence of classes $\{\boldsymbol{E}_k\}$ centered at p_k/q_k that form the steps of one infinite staircase, the symmetry sends the class $\boldsymbol{E}_k$ to $S(\boldsymbol{E}_k)$, where $S(\boldsymbol{E}_k)$ is centered at $(6p_k - q_k)/q_k$. On the z-coordinate, the symmetry can be expressed as the function $S(z) = 6 - 1/z$. In the same three works, the authors proved that, for the staircases being considered, the classes $\{S(\boldsymbol{E}_k)\}$

form the steps of a new[13] infinite staircase. Further, by iterating S, for each positive integer i, $\{S^i(\boldsymbol{E}_k)\}$ is an infinite sequence of classes, which in practice always corresponds to the steps of a new infinite staircase. However, it has not been proven in general that S sends staircases to staircases, and in [Magill and McDuff 2023; Magill et al. 2024; Usher 2019] the authors required specific estimates about the starting $\{\boldsymbol{E}_k\}$ staircases to conclude that, for each i, the $S^i(\boldsymbol{E}_k)$ also form staircases.

For the polydisk, because the function acc is one-to-one, we can also consider the effect of the symmetries on the parameter β of the polydisk via

$$\beta \mapsto \mathrm{acc}^{-1} \circ S \circ \mathrm{acc}(\beta).$$

The transformation on the b-coordinate is the same, but with acc_H replacing acc and its domain restricted to account for the fact that acc_H is two-to-one in general.

In [Magill et al. 2024], it was proved that the images of the four-periodic infinite staircase accumulating to $[\{7, 5, 3, 1\}^\infty]$ under the symmetries also have infinite staircases in their ellipsoid embedding functions. Thus we expect the images of $P\big(1, \frac{1}{12}(6+5\sqrt{30})\big)$ under the Brahmagupta moves likely also have infinite staircases.

Conjecture 4.4.1. *The functions c_{β_i} have infinite staircases, where*

$$\beta_i := \mathrm{acc}^{-1} \circ S^i \circ \mathrm{acc}\big(\tfrac{1}{12}(6+5\sqrt{30})\big).$$

Acknowledgements

We would like to thank the Department of Mathematics at Cornell University for hosting us under the 2022 SPUR program. We also thank Michael Usher for pointing out the relationship between the obstructions $\hat{A}_{i,n}$ and mutation of perfect classes, as well as helpful comments regarding Section 4. We thank the anonymous referee for helpful comments. In addition:

- Caden Farley was supported by Jo Nelson's NSF grant DMS-2104411.
- Tara Holm was supported by NSF grant DMS-2204360.
- Nicki Magill was supported by NSF Graduate Research Grant DGE-1650441.
- Jemma Schroder was supported by the MIT Department of Mathematics.
- Zichen Wang was supported by the Cornell University Department of Mathematics.
- Morgan Weiler was supported by NSF Research Grant DMS-2103245.
- Elizaveta Zabelina was supported by the Nexus Scholars Program in the College of Arts & Sciences, Cornell University.

[13] In the special cases where $\beta = \frac{1}{2}$ or $b = \frac{1}{3}$, when the infinite staircase accumulates to $3+2\sqrt{2}$, the symmetry S actually fixes the staircase, but in all other cases studied a new staircase is found.

Any opinions, findings and conclusions or recommendations expressed in this material are those of the authors and do not necessarily reflect the views of the National Science Foundation.

References

[Bertozzi et al. 2021] M. Bertozzi, T. S. Holm, E. Maw, D. McDuff, G. T. Mwakyoma, A. R. Pires, and M. Weiler, "Infinite staircases for Hirzebruch surfaces", pp. 47–157 in *Research directions in symplectic and contact geometry and topology* (Providence, RI, 2019), edited by B. Acu et al., Assoc. Women Math. Ser. **27**, Springer, 2021. MR Zbl

[Casals and Vianna 2022] R. Casals and R. Vianna, "Full ellipsoid embeddings and toric mutations", *Selecta Math. (N.S.)* **28**:3 (2022), art. id. 61. MR Zbl

[Cristofaro-Gardiner 2019] D. Cristofaro-Gardiner, "Symplectic embeddings from concave toric domains into convex ones", *J. Differential Geom.* **112**:2 (2019), 199–232. MR Zbl

[Cristofaro-Gardiner et al. 2015] D. Cristofaro-Gardiner, M. Hutchings, and V. G. B. Ramos, "The asymptotics of ECH capacities", *Invent. Math.* **199**:1 (2015), 187–214. MR Zbl

[Cristofaro-Gardiner et al. 2017] D. Cristofaro-Gardiner, D. Frenkel, and F. Schlenk, "Symplectic embeddings of four-dimensional ellipsoids into integral polydiscs", *Algebr. Geom. Topol.* **17**:2 (2017), 1189–1260. MR Zbl

[Cristofaro-Gardiner et al. 2020] D. Cristofaro-Gardiner, T. S. Holm, A. Mandini, and A. R. Pires, "On infinite staircases in toric symplectic four-manifolds", 2020. To appear in *J. Differential Geom.* arXiv 2004.13062

[Evans 2023] J. Evans, *Lectures on Lagrangian torus fibrations*, Lond. Math. Soc. Stud. Texts **105**, Cambridge Univ. Press, 2023. MR Zbl

[Frenkel and Müller 2015] D. Frenkel and D. Müller, "Symplectic embeddings of 4-dim ellipsoids into cubes", *J. Symplectic Geom.* **13**:4 (2015), 765–847. MR Zbl

[Hatcher 2022] A. Hatcher, *Topology of numbers*, Amer. Math. Soc., Providence, RI, 2022. MR Zbl

[Hutchings 2011a] M. Hutchings, "Quantitative embedded contact homology", *J. Differential Geom.* **88**:2 (2011), 231–266. MR Zbl

[Hutchings 2011b] M. Hutchings, "Recent progress on symplectic embedding problems in four dimensions", *Proc. Natl. Acad. Sci. USA* **108**:20 (2011), 8093–8099. MR Zbl

[Leung and Symington 2010] N. C. Leung and M. Symington, "Almost toric symplectic four-manifolds", *J. Symplectic Geom.* **8**:2 (2010), 143–187. MR Zbl

[Magill 2024] N. Magill, "Unobstructed embeddings in Hirzebruch surfaces", *J. Symplectic Geom.* **22**:1 (2024), 109–152. MR Zbl

[Magill $\geq$ 2025] N. Magill, "Almost toric fibrations in 2-fold blow ups of $\mathbb{C}\mathrm{P}^2$", in preparation.

[Magill and McDuff 2023] N. Magill and D. McDuff, "Staircase symmetries in Hirzebruch surfaces", *Algebr. Geom. Topol.* **23**:9 (2023), 4235–4307. MR Zbl

[Magill et al. 2023] N. Magill, A. R. Pires, and M. Weiler, "A classification of infinite staircases for Hirzebruch surfaces", preprint, 2023. arXiv 2308.08065

[Magill et al. 2024] N. Magill, D. McDuff, and M. Weiler, "Staircase patterns in Hirzebruch surfaces", *Comment. Math. Helv.* **99**:3 (2024), 437–555. MR Zbl

[McDuff 2009] D. McDuff, "Symplectic embeddings of 4-dimensional ellipsoids", *J. Topol.* **2**:1 (2009), 1–22. Correction in **8**:4 (2015), 1119–1122. MR Zbl

[McDuff 2011] D. McDuff, "The Hofer conjecture on embedding symplectic ellipsoids", *J. Differential Geom.* **88**:3 (2011), 519–532. MR Zbl

[McDuff and Polterovich 1994] D. McDuff and L. Polterovich, "Symplectic packings and algebraic geometry", *Invent. Math.* **115**:3 (1994), 405–434. MR Zbl

[McDuff and Salamon 2017] D. McDuff and D. Salamon, *Introduction to symplectic topology*, 3rd ed., Oxford Univ. Press, 2017. MR Zbl

[McDuff and Schlenk 2012] D. McDuff and F. Schlenk, "The embedding capacity of 4-dimensional symplectic ellipsoids", *Ann. of Math.* (2) **175**:3 (2012), 1191–1282. MR Zbl

[Symington 2003] M. Symington, "Four dimensions from two in symplectic topology", pp. 153–208 in *Topology and geometry of manifolds* (Athens, GA, 2001), edited by G. Matić and C. McCrory, Proc. Sympos. Pure Math. **71**, Amer. Math. Soc., Providence, RI, 2003. MR Zbl

[Usher 2019] M. Usher, "Infinite staircases in the symplectic embedding problem for four-dimensional ellipsoids into polydisks", *Algebr. Geom. Topol.* **19**:4 (2019), 1935–2022. MR Zbl

Received: 2022-12-05 Revised: 2023-08-08 Accepted: 2023-08-12

cfarle10@vols.utk.edu *Department of Mathematics, University of Tennessee, Knoxville, TN, United States*

tara.holm@cornell.edu *Department of Mathematics, Cornell University, Ithaca, NY, United States*

nmagill@berkeley.edu *Department of Mathematics, University of California, Berkeley, California, United States*

jemma@utexas.edu *Department of Mathematics, The University of Texas at Austin, Austin, TX, United States*

zzzichen@umich.edu *Electrical Engineering and Computer Science Department, University of Michigan, Ann Arbor, MI, United States*

morgan.c.weiler@ucr.edu *Department of Mathematics, University of California, Riverside, CA, United States*

ez283@cornell.edu *Department of Mathematics, Cornell University, Ithaca, NY, United States*

involve

msp.org/involve

INVOLVE YOUR STUDENTS IN RESEARCH

Involve showcases and encourages high-quality mathematical research involving students from all academic levels. The editorial board consists of mathematical scientists committed to nurturing student participation in research. Bridging the gap between the extremes of purely undergraduate research journals and mainstream research journals, *Involve* provides a venue to mathematicians wishing to encourage the creative involvement of students.

Cover: Alex Scorpan

See inside back cover or msp.org/involve for submission instructions. The subscription price for 2025 is US $270/year for the electronic version, and $360/year (+$50, if shipping outside the US) for print and electronic. Subscriptions, requests for back issues and changes of subscriber address should be sent to MSP.

Involve (ISSN 1944-4184 electronic, 1944-4176 printed) at Mathematical Sciences Publishers, 798 Evans Hall #3840, c/o University of California, Berkeley, CA 94720-3840, is published continuously online.

Involve peer review and production are managed by EditFlow® from Mathematical Sciences Publishers.

PUBLISHED BY

mathematical sciences publishers

nonprofit scientific publishing

http://msp.org/

involve
2025 vol. 18 no. 1